International Journal of Adhesion & Adhesives 140 (2025) 103978

Contents lists available at ScienceDirect

International Journal of Adhesion and Adhesives

journal homepage: www.elsevier.com/locate/ijadhadh

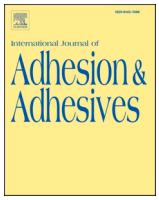

Adhesive geometry dependence of JIS adhesive strength expressed as average stress and countermeasure based on ISSF

Nao-Aki Noda [a,b,**], Rei Takaki [c,*], Yasuaki Suzuki [d], Yasushi Takase [a], Kazuhiro Oda [e]

[a] Mechanical Engineering Department, Kyushu Institute of Technology, 1-1 Sensui-cho, Tobata-ku, Kitakyushu-shi, Fukuoka, 804-8550, Japan
[b] Department of Mechanical Engineering, Indian Institute of Technology Guwahati, North Guwahati, Guwahati, Assam, 781039, India
[c] Department of Mechanical and Electorical Engineering, Nippon Bunri University, 1727 Ichigi, Oita-Shi, Oita, 870-0397, Japan
[d] Suzuki Adhesion Institute of Technology, 131 Aza-yashiki, Ukino, Chiaki-cho, Ichinomiya-shi, Aichi, 491-0806, Japan
[e] Department of Innovative Engineering, Oita University, 700 Dannoharu, Oita-Shi, Oita, 870-1192, Japan

ARTICLE INFO

Keywords:
Adhesive strength
Size effect
Intensity of singular stress field (ISSF)
Elastic modulus
Fracture mechanics

ABSTRACT

The Japanese Industrial Standard (JIS) specifies the adhesive strength as an average ultimate tensile stress without considering the size effect. The prescribed JIS specimen has a smaller adhesive area, $A^{JIS} = (12.7mm)^2$. In this paper, therefore, the reduction of the average adhesive strength is investigated for large adhesive areas $A \gg A^{JIS}$. The discussion is based on the results that the adhesive strength can be expressed as a constant ISSF (Intensity of the Singular Stress Field), as shown in previous studies. Even for ductile resin, the elastic behavior of the adhesive layer is confirmed, as well as small-scale yielding, showing the validity of the ISSF obtained by elastic analysis. Numerical simulation shows that the average adhesive strength varies depending on the adhesive geometry. With a tenfold increase in the adhesive geometry, the adhesive strength decreases to 50 % of the JIS strength, and with a hundredfold increase, the adhesive strength decreases to 20 % of the JIS strength. For large adhesive areas, the JIS strength can be applied by using the same adhesive thickness as that for the small adhesive area specified by the JIS. This is because the ISSF of the actual product is controlled by the adhesive thickness regardless of the adhesive area.

1. Introduction

Adhesive structures, including structural adhesives, offer many advantages such as smooth component surfaces, bonding of dissimilar materials, weight reduction, sealing, and production economics through reduced equipment costs and man-hours. Adhesive bonding technology is becoming increasingly important in the multi-materialization that is key to automotive safety and weight reduction [1,2]. Adhesive bonding technology is becoming increasingly important in multi-materialization, which is key to automotive safety and weight reduction [1,2]. For this reason, numerous studies have been conducted on adhesive joint strength recently [3–26]. These studies focus on nanofillers [3], bi-adhesives [4,5], auxetic adhesives [6], temperature dependence [7], moisture dependence [8], and fatigue crack sensitivity [9]. The authors have dealt with step joints [10] and clarified the improvement of adhesive strength by varying step geometries, considering applications to aerospace due to mechanical efficiency and flat surface requirements [27,28]. Oda et al. [11] have analyzed heat-curing adhesives, assuming interface edge cracks in butt joints, and proposed a useful thermal solution by superposing the results under mechanical and thermal loads.

To evaluate adhesive strength, various test methods are specified by the Japanese Industrial Standard JIS K6848 [29], and the most fundamental tensile adhesive strength is defined as

$$\sigma_c^{JIS} = \frac{P}{A^{JIS}} \tag{1}$$

where $P =$ maximum load, $A^{JIS} =$ adhesive area ($A^{JIS} = W^2 = (12.7mm)^2$).

The adhesive strength σ_c^{JIS} defined in this way varies greatly depending on the thickness h of the adhesive layer. Care should be taken for no description for h in JIS standard and the effect of h is not taken into consideration.

Fig. 1 illustrates test specimens determining (a) tensile strength and yield strength of metals and (b) tensile adhesive strength of bonded butt

* Corresponding author.
** Corresponding author.
E-mail addresses: nao592noda@gmail.com (N.-A. Noda), takakire@nbu.ac.jp (R. Takaki).

https://doi.org/10.1016/j.ijadhadh.2025.103978
Received 26 June 2024; Received in revised form 30 November 2024; Accepted 7 February 2025
Available online 14 February 2025

joint. As shown in Fig. 1, such properties are expressed as average stress. They are applied to various cross sections assuming that the average strength is independent of dimensions of the specimens. Since the round bar in Fig. 1(a) is a smooth specimen with uniform stress, the average stress is useful for determining tensile/yield strength.

The adhesive tensile specimen in Fig. 1 (b) looks smooth but a singular stress field appears at the bonded interface end. In other words, the butt joint looks smooth, but the uneven stress concentration in the adhesive area must be considered. This is the reason why the tensile bond strength σ_c^{JIS} varies depending on the bond thickness h. As the authors have recently pointed out, if the intensity of the singular stress field (ISSF) at the interface end is taken into account, the adhesive strength can be expressed as ISSF = constant independent of h (see Fig. 5 below).

Instead, since the ISSF differs depending on the adhesive area, the tensile adhesive strength σ_c^{JIS} expressed in average stress varies depending on the adhesive area. However, this average adhesive strength σ_c^{JIS} is straightforward, easier to understand than the ISSF, and is widely recognized as adhesive strength. Therefore, this paper discusses the validity of obtaining the tensile adhesive strength $\sigma_c^{W}(h)$ from σ_c^{JIS} specified in JIS when the geometric dimensions of the bonded area are changed, such as when the bonded area is larger than the JIS bonded area $A = W^2 > (12.7mm)^2$. The discussion of ISSF is based on elastic analysis. Therefore, the elastic behavior of the adhesive layer will be considered even when commonly used ductile adhesives are used. The plastic zone size generated in the adhesive layer satisfies the small-scale yield condition, which will be confirmed even at the maximum load by changing the geometry of the adhesive layer.

2. Adhesive strength prescribed in JIS standards and variation depending on adhesive geometry

As described above, various test methods for evaluating adhesive strength are specified by the Japanese Industrial Standard JIS K6848 [29], and tensile adhesive strength is defined in Equation (1) as an average adhesive strength. Also, JIS K6849 [30,31] described the detail of the testing method.

Fig. 2 shows the critical remote tensile stress σ_c^{JIS} experimentally obtained [32–34] following the description of the testing method in JIS standard by varying the adhesive layer thickness h. The results for five different adhesive/adherend material combinations are indicated, that is, ① Resin A/S35C, ② Resin B/S35C, ③ Araldite/Al, and ④ Solder/-Brass, ⑤ Shell epon 828/Aluminum. The solid circles denote the average values of experimental results. Table 1 shows mechanical properties of these materials.

Fig. 2 also indicates bulk adhesive strength σ_B^{Bulk} for ①~④ for comparison. Although the bulk adhesive strength of ⑤ is unknown, the main component is almost the same as that of the adhesive in ② in Ref. [32], and the bulk strength ⑤ is almost the same as that of the one of ②. From the comparison between the butt joint strength and the bulk strength, it can be seen that the butt joint strength can be sometimes larger than the bulk strength as can be seen for ductile adhesives ②, ④, ⑤ as $\sigma_c^{Butt} \rangle \sigma_B^{Bulk}$. This is because such adhesive layers are strongly constrained by the adherend to deform in the $x-$ and the $z-$ directions and behave elastic as explained in Section 3.

As shown in Fig. 2, it is well known that σ_c^{JIS} varies significantly depending on h. For example, σ_c^{JIS} = 76.8–13.6 MPa when S35C is bonded with Resin B, which can be regarded as common commercial adhesives. Even when the adhesive layer thickness $h = 0.05 \sim 0.6mm$ commonly used, it varies as σ_c^{JIS} = 76.8–35.7 MPa. Therefore, all σ_c^{JIS} should be expressed at least as a function of h, $\sigma_c^{JIS} = \sigma_c^{JIS}(h)$. However, there is no description of the adhesive layer thickness h in the JIS standard, and it is not taken into account [29]. In addition, in JIS standard, there are no descriptions referring to the relationship between the adhesive layer thickness h and adhesive strength. In other standards such as ASTM and ISO, or in adhesive technology textbooks [31,35–38], there are no descriptions referring to the relationship between the critical remote tensile stress σ_c and the adhesive layer thickness h. One may think that controlling the adhesive layer thickness h is difficult, but the following method can be applied to make the adhesive layer thickness h in the JIS test specimen [39] (see Section 9).

In other JIS testing methods such as adhesive shear strength using lap joints and so on, the adhesive strength is also defined as the maximum load divided by the adhesive area [29]. For example, the adhesive strength of lap joint is defined as $\tau_c^{JIS} = N/A$, where N = maximum load, A = adhesive area (A = 12.5 × 25 mm^2). Fig. 3 shows an example of adhesive strength τ_c by varying the adhesive area $A = l_b \times 25$ mm when Aluminum is bonded by brittle epoxy resin [40]. The average strength of lap joints is insensitive to the adhesive layer thickness h, but as shown in Fig. 3, the adhesive strength τ_c varies significantly depending on the bond length l_b. In this way, if the adhesive strength expressed as

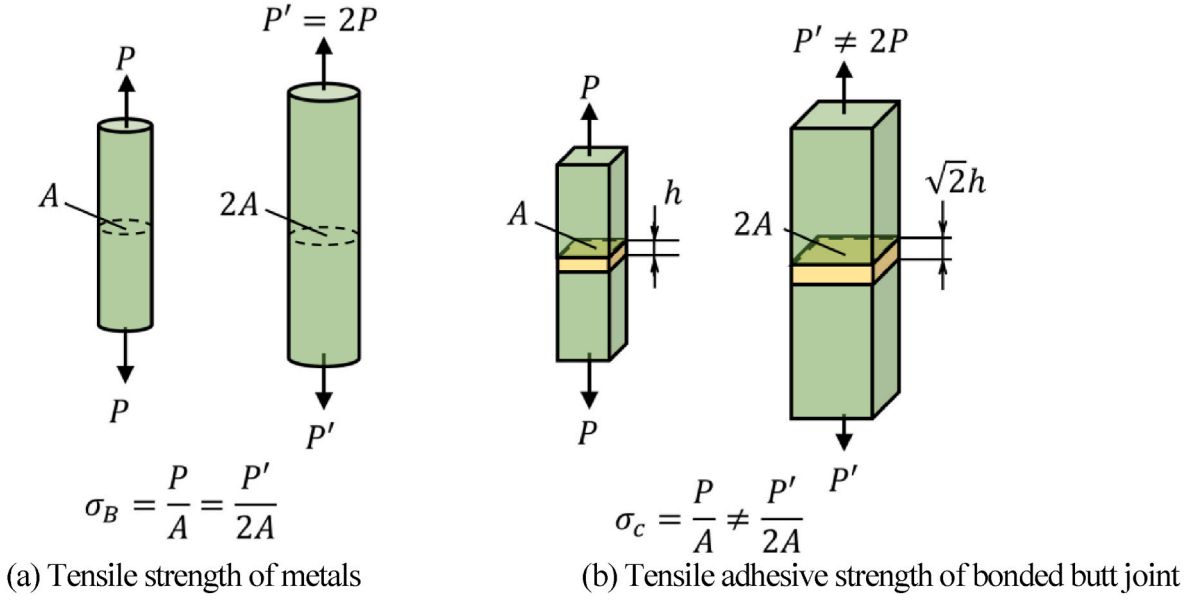

Fig. 1. Illustration of tensile strength σ_B and tensile adhesive strength σ_c for the similarity ratio $\sqrt{2}$

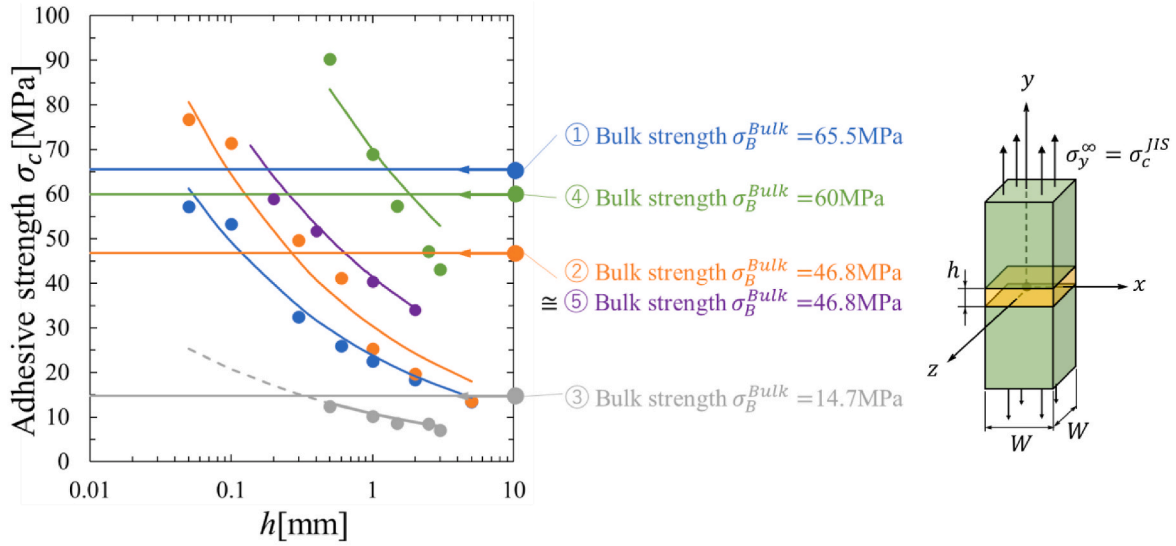

(a) Butt joint adhesive strength expressed as $\sigma_c^{JIS} = P/A$ (P = ultimate tensile load, $A = W^2$ = fixed adhesive area) varying depending on adhesive layer thickness h

(b) Prismatic butt joint geometry with $W = 12.7mm$ (JIS) [32-34] for ①, ②, $W = 10mm$ for ③, ④ and $W = 28.6mm$ for ⑤.

Fig. 2. Experimentally obtained butt joint strength $\sigma_c^{JIS} = P/A$ in comparison with bulk adhesive strength σ_B^{Bulk} ① $\sigma_c = (0.934 \sim 0.219)\sigma_B^{Bulk}$ for Resin A/S35C, σ_B^{Bulk} = 65.5 MPa, ② $\sigma_c = (1.715 \sim 0.382)\sigma_B^{Bulk}$ for Resin B/S35C, σ_B^{Bulk} = 46.8 MPa,③ $\sigma_c = (0.741 \sim 0.541)\sigma_B^{Bulk}$ for Araldite/Al, σ_B^{Bulk} = 14.7 MPa, ④ $\sigma_c = (1.164 \sim 0.880)\sigma_B^{Bulk}$ for Solder/Brass, σ_B^{Bulk} = 60.0 MPa ⑤ $\sigma_c = (1.366 \sim 0.737)\sigma_B^{Bulk}$, Shell epon 828/Aluminum, σ_B^{Bulk} = 46.8 MPa.

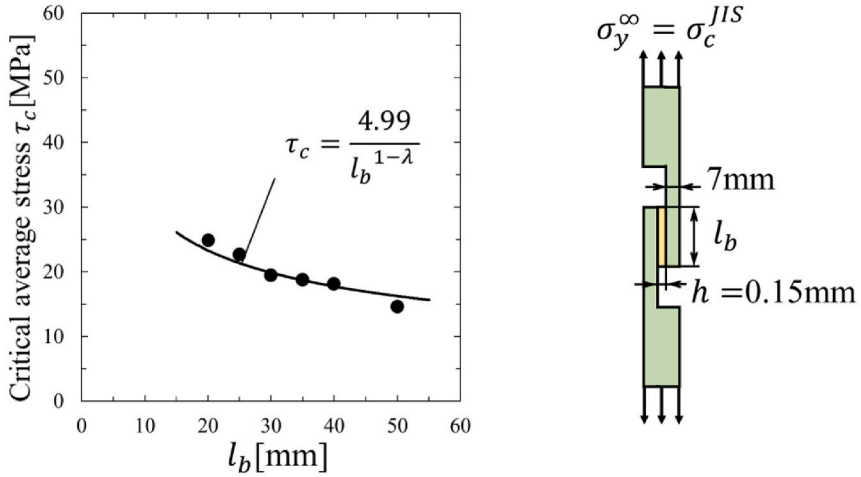

(a) Adhesive strength expressed as $\tau_c = N/A$ (N =ultimate tensile load, A =adhesive area $= l_b \times 25mm$)

(b) Lap joint geometry with A =adhesive area= $l_b \times 25mm$

Fig. 3. Lap joint adhesive strength expressed as $\tau_c = N/A$, P = ultimate tensile load, A = adhesive area under fixed $A = l_b \times 25mm$ when Aluminium is bonded by brittle epoxy resin [40] (τ_c = 24.8–14.6 MPa).

maximum load/adhesive area, i.e., average stress, care should be taken for $\sigma_c^{JIS} = P/A$ and $\tau_c^{JIS} = N/A$ vary depending on the adhesive layer geometries.

As shown in Fig. 3, the adhesive strength $\sigma_c^{JIS}(h)$ specified in JIS has another problem in that it does not take into account the effect of the adhesive area $A = W^2$. Usually, a larger area A is bonded for practical use than the area specified in JIS as $A > A^{JIS} = (12.7)^2 mm^2$. However, it is not clear whether the average stress $\sigma_c^{JIS}(h)$ obtained by JIS when $A = (12.7)^2 mm^2$ is still applicable to the adhesive strength $\sigma_c^{W}(h)$ as can be expressed as $\sigma_c^{W}(h) = \sigma_c^{JIS}(h)$, or whether $\sigma_c^{W}(h) < \sigma_c^{JIS}(h)$.

3. Adhesive strength of a butt joint expressed as a constant ISSF and tensile strength of a cracked plate expressed as a constant SIF

Regarding the singular stress appearing at the interface edge, many useful analyses were performed to obtain the singularity index and the eigenfunction [41–44]. Then, the adhesive strength was discussed based on these analyses [45–47]. The authors used the term "ISSF (Intensity of Singular Stress Field)" for people to understand the meaning in straightforward, then demonstrating that the adhesive strength can be expressed as ISSF = constant for various combinations of adhesives and adherends (see Fig. 5) [48–52]. The outline of the analysis method named "mesh-independent proportional method" to obtain the ISSF is

Table 1
Material properties for Adhesive/Adherend.

Material	Young's modulus E_y^{Resin} [GPa] E_y^{Steel} [GPa]	Poisson's ratio ν	Bulk strength σ_B [MPa]	Dundurs parameter α	β
				Singularity index λ	
① Resin A/	3.14	0.37	65.5	0.969	0.199
S35C	205.9	0.30	570	$\lambda = 0.685$	
② Resin B/	2.16	0.38	46.8	0.978	0.188
S35C	205.9	0.30	570	$\lambda = 0.674$	
③ Araldite/	2.1	0.36	14.8	0.941	0.205
Al	70	0.35	260	$\lambda = 0.714$	
④ Solder/	6.4	0.39	60	0.862	0.151
Brass	90	0.34	205	$\lambda = 0.745$	
⑤ Shell epon 828/	3.6	0.35	–	0.902	0.207
Al	70	0.35	260	$\lambda = 0.732$	

indicated in Appendix A for the readers' convenience. In this study, the FEM software MSC software's Marc/Mentat 2019 was used for this elastic analysis. In this code, the complete Newton–Raphson strategy is used to solve non-linear equations in an implicit scheme [53]. Here, a 4-node quadrilateral plane strain element is used with the number of mesh elements are 2.2×10^6. The validity of the elastic analysis will be shown in the following Section 4 and Section 5 for ductile resin.

Consider a prismatic butt joint prescribed in JIS standard as shown in Fig. 2 whose interfaces are $y = \pm h/2$. At the interface end $(x,z) = (x, \pm W/2)$ or $(\pm W/2, z)$, the singular stress field can be expressed in Equation (2) where r is the distance from adhesive interface edge, and λ is the singularity index and $K_\sigma^{Side}(x,z)$ is the ISSF.

$$\sigma_y^{Side}(x,z) \to \frac{K_\sigma^{Side}(x,z)}{r^{1-\lambda}} \quad (r \to 0), \qquad (2)$$

$(x,z) = (x, \pm W/2)$ or $(\pm W/2, z)$ in Figure 3 (b)

The notation λ in Eq. (2) denotes the singularity index, and values can be determined from Eq. (A3) in Appendix A. The ISSF $K_\sigma^{Side}(x,z)$ in Fig. 3(b) can be calculated by applying the same mesh pattern to unknown and reference problems because they have proportional singular stress fields [48–52,54]. The detail was indicated in Refs. [51,52,54] and for the readers' convenience the outline of the analysis method is indicated in Appendix A. Then, Fig. 4 shows that the adhesive strength can be expressed as a constant ISSF as $K_{\sigma c}^{Side}(0) = 1.227 \pm 0.164 [\mathrm{MPa} \bullet \mathrm{m}^{0.326}]$ for ② Resin B/S35C in Table 1 [51].

Compared to the 3D FEM analysis of the prismatic butt joint in Fig. 2, it is much easier to perform a 2D FEM analysis of the plate butt joint under plane strain. Therefore, Fig. 4 also shows the constant ISSF $K_{\sigma c}^{2D} = 1.204 \pm 0.172 [\mathrm{MPa} \bullet \mathrm{m}^{0.326}]$ obtained by analyzing the plate butt joint under plane strain. It is seen that the results of the 2D and 3D analyses are identical. Confirms the usefulness of the simple two-dimensional analysis, Fig. 2 includes the relation $\sigma_c^{JIS}(h) = 3.18/h^{1-\lambda}$, which can be obtained from $K_{\sigma c}^{2D} = 1.204 \pm 0.172 [\mathrm{MPa} \bullet \mathrm{m}^{0.326}]$.

Focusing on the corner $(x,z) = (\pm W/2, \pm W/2)$, Fig. 4 also shows that the constant corner ISSF as $K_{\sigma c}^{Corner} = 0.595 \pm 0.138 [\mathrm{MPa} \bullet \mathrm{m}^{0.404}]$. In terms of the singularity exponent, there is a stronger singular field at the corner than at other interface edge as $0.404 > 0.326$. However, since the range is limited, and the specimen's corners are usually chamfered, it was confirmed that adhesive debonding occurs at interface edges other than at corners. Fig. 4 indicating that the adhesive strength can be expressed by one of the critical ISSFs. In the following discussion, therefore, by using the 2D constant ISSF $K_{\sigma c}^{2D} = 1.204 [\mathrm{MPa} \bullet \mathrm{m}^{0.326}]$, the variation of the critical strength σ_c^W depending on adhesive geometry will be discussed.

Similar to Figs. 4 and 5 (a) summarizes the constant ISSFs of the butt joints for ① Resin A/S35C, ② Resin B/S35C, ③ Araldite/Al, ④ Solder/Brass. Using these constant values in Fig. 5, the curves ① $\sigma_c = 2.70/h^{1-\lambda}$ (Resin A/S35C), ② $\sigma_c = 3.18/h^{1-\lambda}$ (Resin B/S35C), ③ $\sigma_c = 1.51/h^{1-\lambda}$ (Araldite/Aluminum), ④ $\sigma_c = 12.0/h^{1-\lambda}$ (Solder/Brass), ③ $\sigma_c = 6.52/h^{1-\lambda}$ (Shell epon 828/Aluminum) can be obtained and indicated in Fig. 2. For each material combination ①~⑤, the debonding strength can be expressed as a constant ISSF within about 10 % error. It should be noted that those curves are extended to the region where no experimental results. For example, as shown in Fig. 2 (a), for ③Araldite/Aluminum, experimental results are available only in the range 0.5 mm $\le h \le$ 3 mm but the results $\sigma_c = 1.51/h^{1-\lambda}$ can be extended to the range $h \le 0.5$ mm as indicated in dashed line in Fig. 2. Such adhesive strength prediction based on the constant ISSF will be discussed in Section 7 in detail. The prediction can be provided to other joints. As an example, regarding the lap joint in Fig. 3 (b), the curve $\tau_c = 4.99/{l_b}^{1-\lambda}$ is obtained from the ISSF = constant and indicated in Fig. 3 (a).

A butt joint appears to be a smooth specimen with no stress concentration. Therefore, it may be difficult for some people to understand that the adhesive strength is expressed in terms of a constant ISSF rather than a prescribed average stress in JIS. Similar situation has been

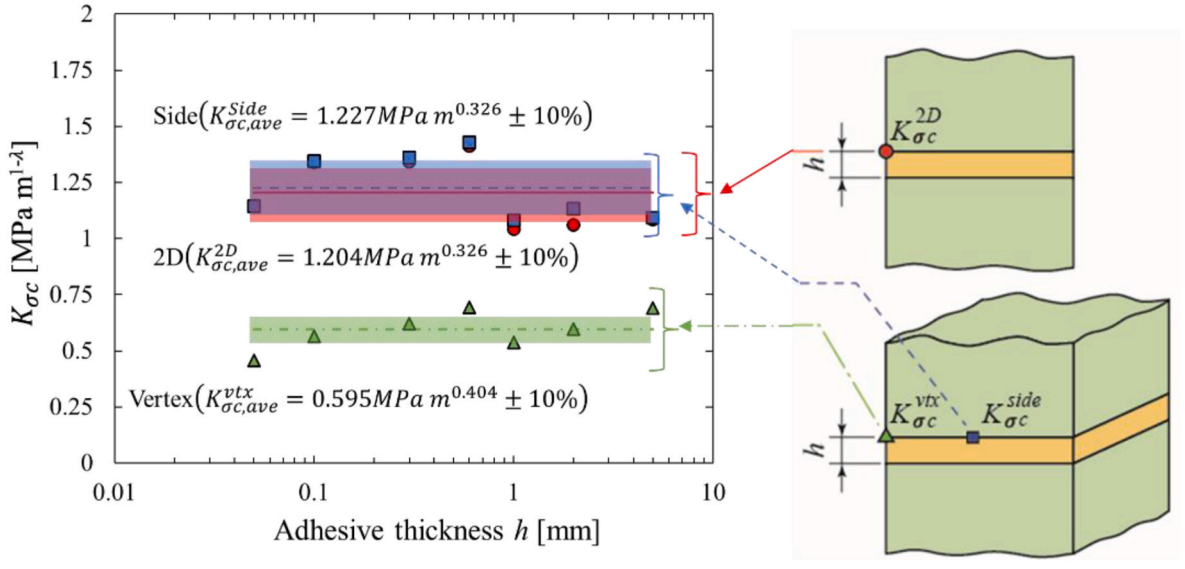

Fig. 4. Prismatic butt joint strength for ② in Table 1 can be expresses as ISSF = constant obtained by the two-dimensional FEM analysis.

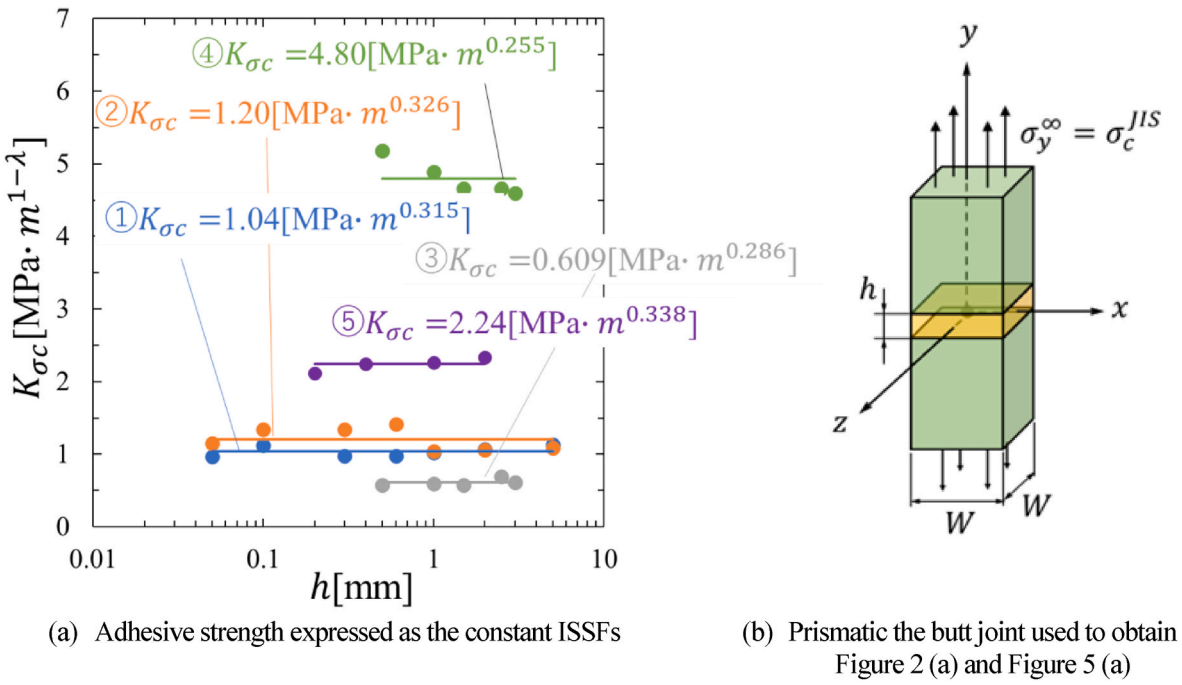

(a) Adhesive strength expressed as the constant ISSFs (b) Prismatic the butt joint used to obtain Figure 2 (a) and Figure 5 (a)

Fig. 5. Butt joint strength in Fig. 2 can be expresses as constant ISSF for ①~⑤ in Fig. 2.

experienced in past research in the field of fracture mechanics. It is well known today that the brittle fracture strength of a cracked body can be expressed as a constant stress intensity factor K, which corresponds to the ISSF of the crack. Fig. 6 shows the relationship between the fracture stress σ_c and the stress intensity factor at failure K_{Ic} and the relative crack length a/W for a flat plate with an edge crack [55]. The fracture stress σ_c decreases with increasing relative crack length a/W, while the stress intensity factor K_{Ic} is constant and independent of a/W. The relationship between the adhesive layer thickness h and the ISSF in the butt joint shown in Fig. 5 is similar to the relationship between the crack length "a" and the stress intensity factor K in the cracked plate shown in Fig. 6. In the case of butt joints, the thickness h of the adhesive layer corresponds to the crack length a. There is a slight difference between the two. The crack material in Fig. 6 has one singular field at the crack tip, whereas the butt joint has two singular fields at the upper and lower adhesive edges. Therefore, the crack length "a" in the cracked plate in Fig. 6 and h in the butt joint in Fig. 5 behave similarly to the crack length "a" because the ISSF is reduced by the interaction when h is small. Thus, unlike the crack length "a", the adhesive layer thickness h is a quantity related to the interaction effect of the singular fields at the two points above and below the bonded edge, so that for $h/W \geq 1$, the ISSF is constant since there is no interaction. In other words, the effect of the adhesive layer thickness h on the ISSF (interference effect) is similar to the effect of the stress intensity factor K, which varies with distance h when two parallel cracks of the same length and distance h exist in the cracked plate in Fig. 6.

When the average stress $\sigma_c^{JIS} = P/A$ is used to evaluate the adhesive strength of butt joints, if the adhesive layer thickness h is sufficiently large ($h/W \geq 1$), then the ISSF is constant and independent of h because there is no singularity interaction anymore. Therefore, the adhesive strength can be evaluated by using σ_c^{JIS} (see Fig. 9 below). In reality, however, h = 0.05–0.6 mm is the practical range of adhesive layer

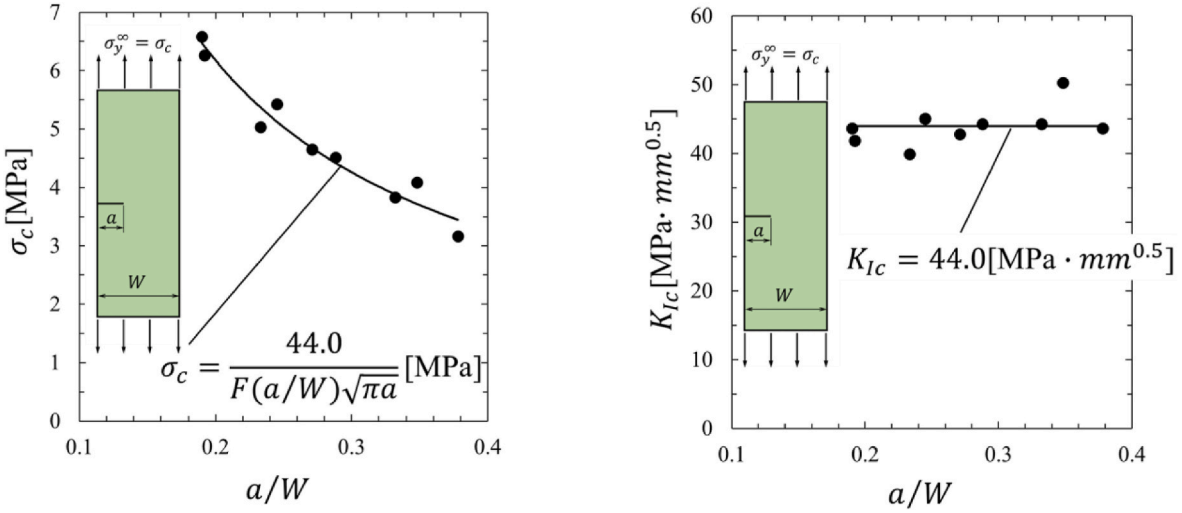

Fig. 6. Fracture strength of an edge cracked acrylic resin plate, which can be expressed as a constant stress intensity factor K_{Ic} although σ_c varies depending on the crack length a/W [55].

thickness, so the use of ISSF is necessary. Furthermore, even if $h/W \geq 1$ is satisfied, the ISSF varies depending on the adhesive area ($A = W^2$) as shown in Fig. 9 below; and therefore, $\sigma_c^{JIS} = P/A$ varies depending on W.

4. Elastic behavior of the adhesive layer in butt joint

In Fig. 7(a), $\sigma_y^\infty - \varepsilon_y^{Bulk}$ shows the stress-strain relation of bulk adhesive Resin B, which is measured according to ASTM D638 [56]. Considering previous studies to analyze the bulk adhesive by using FEM, the elastic-perfectly plastic solid is assumed as shown in the dashed line $\sigma_{yield}^{Bulk} = \sigma_B^{Bulk} = 46.8$ MPa in FEM analysis. The stress-strain curve of bulk epoxy Resin B has a clear yield point and ductile fracture strain $\varepsilon_f \approx 8\,\%$. Resin B does not use any additives and the ductile resin properties are controlled by the mixing ratio of brittle and ductile resins. Instead, to increase ductility, commercial adhesives often use additives such as rubber particles flexible curing agents, or plasticizers. The stress-strain relation of Resin B epoxy is close to that of many commercially available adhesives; and therefore, the discussion in this paper is applicable to adhesives used in practical applications. Therefore, the following discussion mainly focuses on Resin B/S35C in Table 1.

To compare with the bulk adhesive $\sigma_y^\infty - \varepsilon_y^{Bulk}$, Fig. 7(a) also shows the adhesive layer's relation $\sigma_y^\infty - \varepsilon_y^{Resin}$ for various h [56]. The relation $\sigma_y^\infty - \varepsilon_y^{Resin}$ is obtained from the strain ε_y^{Joint} obtained by the strain gauge whose length $l = 5$ mm affixed across the adhesive layer (see Fig. 7). Since this strain ε_y^{Joint} includes the adherend strain $\varepsilon_y^{Steel} = \sigma_y^\infty / E_{Steel}$, the

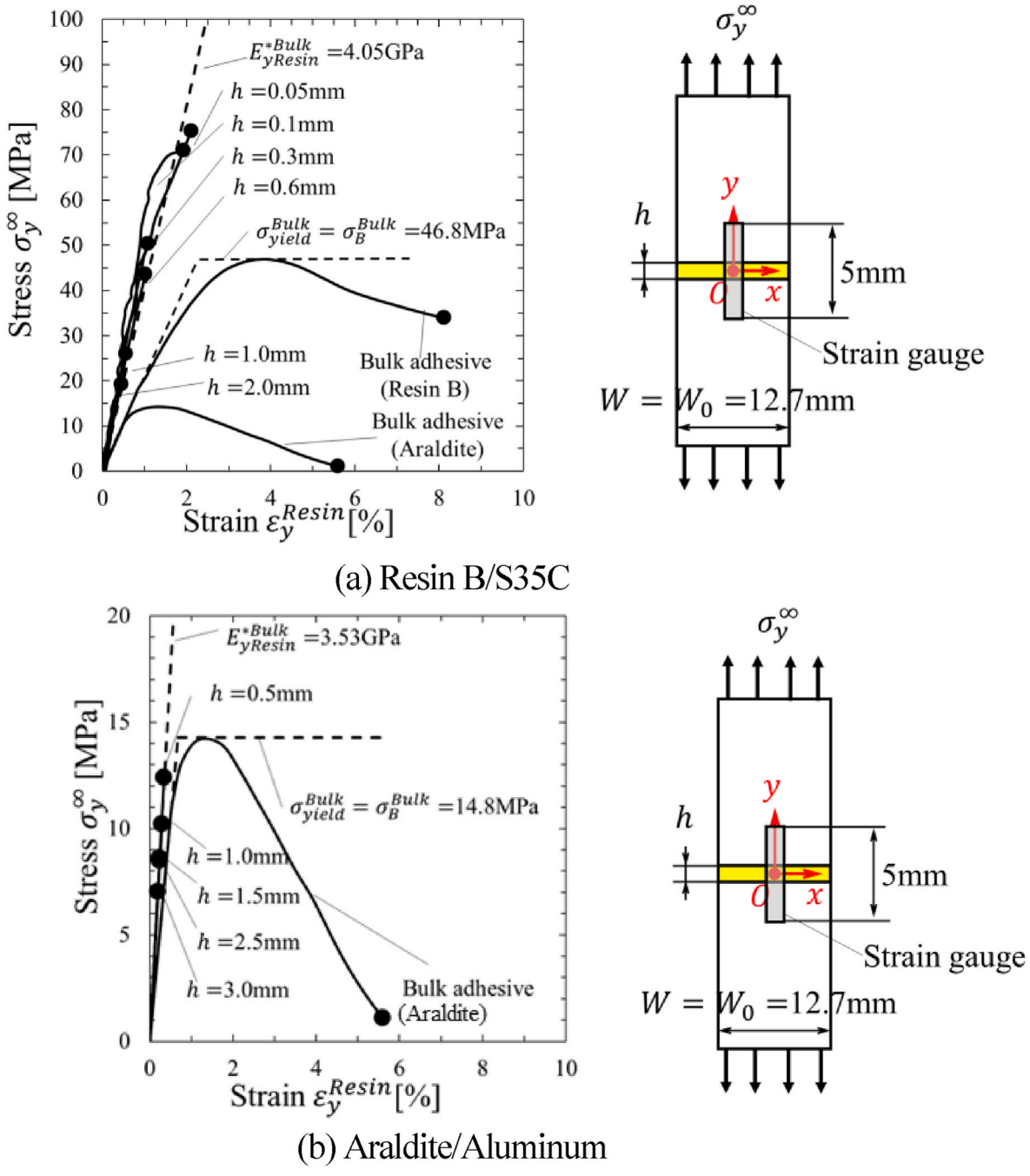

Fig. 7. Stress-strain relation $\sigma_y^\infty - \varepsilon_y^{Resin}$ of adhesive layer in butt joint for (a) Resin B/S35C and (b) Araldite/Aluminum in Table 1 in comparison with the bulk adhesive relation $\sigma_y^\infty - \varepsilon_y^{Bulk}$

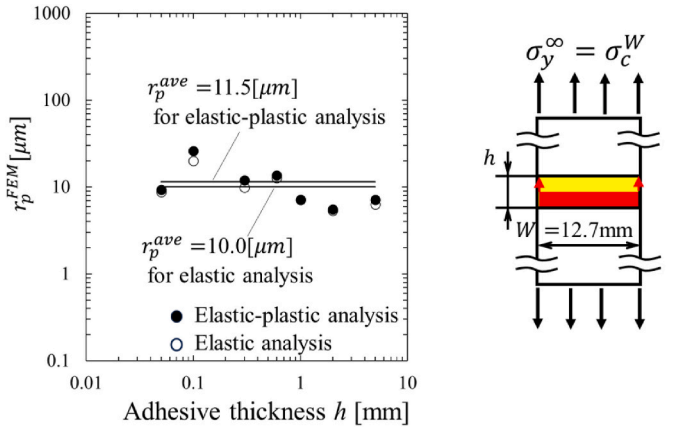

Fig. 8. Plastic zone size r_p obtained by FEM analysis.

average strain ε_y^{Resin} of the adhesive layer itself is obtained by removing ε_y^{Steel} from ε_y^{Joint} as shown in Equation (3). In Equation (3), $l_{Steel}(=l-h)$ is the length of the portion of the strain gage attached to the adherend, and E_{Steel} is Young's modulus of the adherend.

$$\varepsilon_y^{Resin}=\frac{l}{h}\left(\varepsilon_y^{Joint}-\varepsilon_y^{Steel}\frac{l_{Steel}}{l}\right)=\frac{l}{h}\left(\varepsilon_y^{Joint}-\frac{\sigma_y^\infty}{E_{Steel}}\frac{l_{Steel}}{l}\right) \tag{3}$$

As shown in Fig. 7(a), the relations $\sigma_y^\infty-\varepsilon_y^{Resin}$ and $\sigma_y^\infty-\varepsilon_y^{Bulk}$ are totally different. This is because the adhesive layer is strongly constrained by the adherend to deform in the $x-$, $z-$ directions. As shown in Equation (4), the virtual Young's modulus is obtained as $E_y^{*Resin}=1.87E_y^{Resin}=4.05GPa$, which can be derived by applying the stresses $\sigma_x=\sigma_z=\nu/(1-\nu)\sigma_y^\infty$ in the $x-$, $z-$ directions together with the stress σ_y^∞ so as to satisfy $\varepsilon_x=\varepsilon_z=0$. Quite different from E_y^{Resin} in Table 1, $E_y^{*Resin}=4.05GPa$ is indicated as a dashed line in Fig. 7(a).

$$E_y^{*Resin}=\frac{1-\nu}{(1-2\nu)(1+\nu)}E_y^{Resin}=4.05GPa \tag{4}$$

As shown in Fig. 7(a), the experimentally obtained stress-strain relations of the adhesive layer $\sigma_{y0}-\varepsilon_y^{Resin}$ [32] are linear and elastic for $h=$ 0.05~2 mm. Their slopes approximately coincide with the slope of the dashed line indicated in Fig. 7, that is, $E_y^{*Resin}=4.05GPa$ in Equation (4). To determine the average Young's modulus of the adhesive layer more accurately, an elastic-plastic analysis is performed for the butt joints of ②Resin B/S35C by using FEM. Then, it is confirmed that the average Young's modulus of the adhesive layer agrees with $E_y^{*Resin}=4.05GPa$ in Equation (4) within a few percent except for the extremely thick adhesive layer thickness $h=5$ mm.

As shown in Fig. 7(a), the adhesive strength $\sigma_y^\infty=\sigma_c$ exceeds the bulk adhesive strength $\sigma_B^{Bulk}=46.8$ MPa when $h\le 0.3$ mm. The stress-strain relationship $\sigma_{y0}-\varepsilon_y^{Resin}$ of the adhesive layer is almost linear up to fracture without showing yield point. Unlike the bulk adhesive strain at final fracture $\varepsilon_f\approx 8$ %, the strain of the adhesive layer at final fracture ε_f is only $\varepsilon_f=0.5$–2 %. Even when $h=0.05$ mm where ε_f is the largest, the relations $\sigma_{y0}-\varepsilon_y^{Resin}$ is almost elastic until $\varepsilon_f\approx 2$ %.

In Fig. 7(b), $\sigma_y^\infty-\varepsilon_y^{Bulk}$ shows the stress-strain relation of bulk adhesive of Araldite. Considering previous studies to analyze the bulk adhesive, the elastic-perfectly plastic solid is assumed as shown in the dashed line $\sigma_{yield}^{Bulk}=\sigma_B^{Bulk}=14.8$ MPa in this FEM analysis. The stress-strain curve for the epoxy resin Araldite shows a clear yield point and ductile fracture strain $\varepsilon_f\approx 6$ %. Araldite is a widely used commercial adhesive and is representative of other commercial adhesives although the strength is relatively low. Therefore, the discussion of Araldite/Aluminum can be applied to other adhesives used in practical applications. The following discussion focuses on ③Araldite/Aluminum in Table 1 and discusses the elastic behavior of the adhesive layer.

As shown in Fig. 7(b), the experimentally obtained stress-strain relations of the adhesive layer $\sigma_{y0}-\varepsilon_y^{Resin}$ are linear and elastic for $h=$ 0.5–3.0 mm. Their slopes approximately coincide with the slope of the dashed line indicated in Fig. 7, that is, $E_y^{*Resin}=3.53$GPa in Equation (4).

As shown in Fig. 7(b), the adhesive strength $\sigma_y^\infty=\sigma_c$ does not exceed the bulk adhesive strength $\sigma_B^{Bulk}=14.8$ MPa. The stress-strain relationship $\sigma_{y0}-\varepsilon_y^{Resin}$ of the adhesive layer is almost linear up to fracture without showing yield point.Unlike the bulk adhesive strain at final fracture $\varepsilon_f\approx 6$ %, the strain of the adhesive layer at final fracture ε_f is only $\varepsilon_f\approx 0.20$–0.35 %.

5. Plastic zone size of the adhesive layer in butt joint

The adhesive strength σ_c^W discussed in the following sections of this paper is based on ISSF obtained by elastic analysis. Although the elastic behavior of the adhesive layer has already been clarified, in this section the plastic zone size of the adhesive layer will be discussed to demonstrate the validity of the elastic analysis. Following the previous studies [57,58], the adhesive is assumed to be elastic-perfectly plastic solid in this FEM analysis, as shown by the dashed line in Fig. 7. Since the yield stress of the adherend such as S35C is sufficiently high compared to that of the adhesive, it can be treated as an elastic body. In this study, the FEM code MSC Marc/Mentat 2019 was used for the simulation of the size effect of butt joint based on the previous results that the adhesive

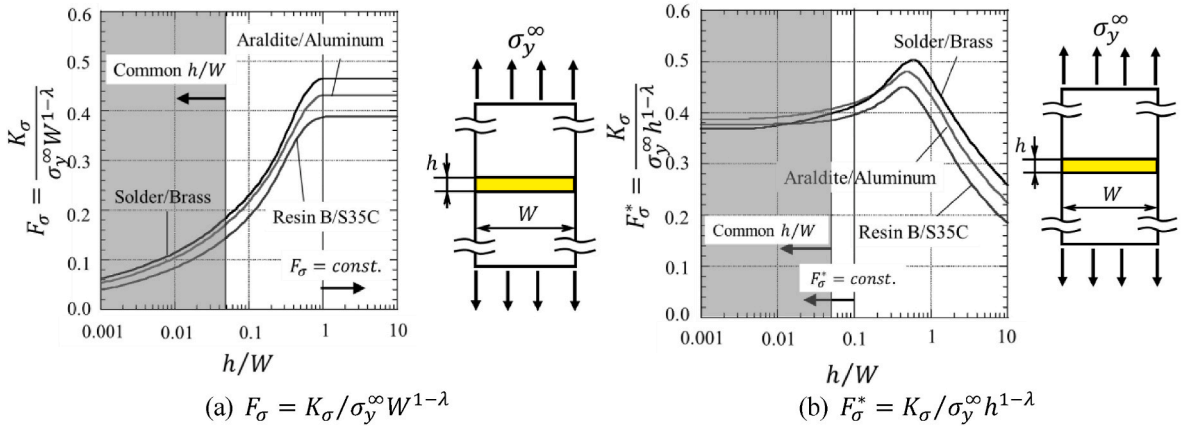

Fig. 9. Dimensionless ISSF defined as (a) $K_\sigma=F_\sigma(h/W)\sigma_y^\infty W^{1-\lambda}$ and (b) $K_\sigma=F_\sigma(h/W)\sigma_y^\infty h^{1-\lambda}$, $\sigma_y(r)\to K_\sigma/r^{1-\lambda}$ $(r\to 0)$ for butt joints whose material combination are Resin B/S35C, Araldite/Aluminum and Solder/Brass.

strength can be expressed as a constant ISSF.

Fig. 8 shows the plastic zone of the butt joint the r_p^{FEM} obtained by the elastic-plastic analysis under the critical stress $\sigma_y^{\infty} = \sigma_c$. As shown in Fig. 8, the size of the plastic zone is nearly constant independent of the thickness of the adhesive layer h. The average value $r_p^{ave} = 11.5\mu m$ is much smaller than the specimen width W and satisfy the small-scale yielding condition. Even when the adhesive strength exceeds the bulk strength $\sigma_c > \sigma_B^{Bulk}$, the plastic zone size r_p^{FEM} is sufficiently smaller. Fig. 8 also shows the plastic zone size $r_p^{ave} = 10.0\mu m$ determined from elastic analysis assuming the region where the elastic Mises stress is larger than the yield stress. It is seen that two results $r_p^{ave} = 11.5\mu m$ and $r_p^{ave} = 10.0\mu m$ agree within an error of 15 %. Small-scale yielding indicates that the ISSF based on elastic analysis is valid and useful even for ductile resin B. Therefore, based on the ISSF, it is possible to discuss the adhesive strength when the shape of the adhesive layer is changed.

6. Variation of ISSF depending on adhesive geometry in butt joints and dimensionless ISSF F_σ and F_σ^* to express ISSF

The ISSF in the butt joint varies depending on the adhesive layer geometry. Therefore, the authors proposed two types of dimensionless ISSF for the users' convenience. In the previous studies [48,59], first, the expression $F_\sigma(h/W) = K_\sigma/(\sigma W^{1-\lambda})$ was considered as the ISSF K_σ normalized by using the average tensile stress $\sigma_y^{\infty} = \sigma$ and the specimen width W in Equation (5). Next, the expression $F_\sigma^*(h/W) = K_\sigma/\left(\sigma h^{1-\lambda}\right)$ was considered as the ISSF K_σ normalized by using the average tensile stress $\sigma_y^{\infty} = \sigma$ and the thickness of the adhesive layer normalized by using the average tensile stress $\sigma_y^{\infty} = \sigma$ and specimen width W in Equation (6).

$$F_\sigma(h/W) = \frac{K_\sigma}{\sigma_y^{\infty} W^{1-\lambda}} \tag{5}$$

$$F_\sigma^*(h/W) = \frac{K_\sigma}{\sigma_y^{\infty} h^{1-\lambda}} \tag{6a}$$

Fig. 9(a) shows the variation of $F_\sigma(h/W)$ in Equation (5) obtained by the proportional method [50–52]. The outline of this analysis method is indicated in Appendix A. The dimensionless ISSF $F_\sigma(h/W)$ is depending on only h/W. If different adhesive geometries have the same h/W, they have the same $F_\sigma^*(h/W)$. As shown in Fig. 9 (a), with decreasing the adhesive layer thickness h, $F_\sigma(h/W)$ decreases. This is due to the interaction of the singular points located above and below of the end of the adhesive layer interface. This is the reason why σ_c^{JIS} increases with decreasing h as shown in Fig. 2, and the adhesive strength is expressed as a constant ISSF as shown in Fig. 5. The ISSF F_σ in Equation (5) becomes constant when $h/W \geq 1$. This can be explained by Saint-Venent's principle.

Conversely, as shown in Fig. 9(b), the expression $F_\sigma^*(h/W)$ in Equation (6) becomes constant when $0 \leq h/W \leq 0.1$. This is extremely useful for evaluating adhesive joint strength. This is because the practical adhesive thickness is in the range $h = 0.05 \sim 0.6mm$, and the adhesive dimension is usually larger than the one in JIS specimen as can be expressed $W \geq 12.7mm$. Therefore, the region $h/W \leq 0.0472$ can be the practical range of adhesive layer thickness, and the indication of $F_\sigma^*(h/W)$ gives constant values within this range, as shown in Fig. 9(b). For example, for Resin B/S35C, $F_\sigma^*(h/W) \approx$ constant ≈ 0.377 (see Eq. (6b)), and for other material combinations, $F_\sigma^*(h/W) \approx$ constant, as well.

$$F_\sigma^*(h/W) = \frac{K_\sigma}{\sigma_y^{\infty} h^{1-\lambda}} \approx \text{constant} \approx 0.377 \tag{6b}$$

for Resin B/S35C when $0 \leq h/W \leq 0.1$

7. Formula of F_σ^* to provide ISSF under arbitrary metal/resin combination

Table 2 and Fig. 10 show the value of F_σ^* under arbitrary material combination for $h/W \leq 0.1$ for the entire range of Dundurs' parameters (see Equation (A1) in Appendix A). From Fig. 10, assuming that the adhesive layer thickness h of the actual adhesive joint is in the range $0.05 \leq h \leq 0.6$ mm, the tensile adhesive strength for practical use can be evaluated by finding the F_σ^* for $0.05 \leq h \leq 0.6$ mm. Regarding the JIS specimen, since the width $W = 12.7$ mm is specified, h/W is in the range $0.00394 \leq h/W \leq 0.0472$. Usually, in practice, the adhesive area is much larger, the range of $h/W \leq 0.0472$ should be considered. Therefore, the constant value of F_σ^* can be applied since they are in the range $0 \leq h/W \leq 0.1$. Under arbitrary metal/resin combination, F_σ^* is in the range $F_\sigma^* = 0.3$–0.6, the practical adhesive strength can be evaluated using this range.

Table 3 summarizes F_σ^* for steel/resin and aluminum alloy/resin combinations discussed in the previous studies. In Table 3, F_σ^* is obtained from α, β from the resin's Young's modulus E^{Resin} and Poisson's ratio ν^{Resin} when steel and aluminum alloy are adherend [60]. As shown in Table 3, the values of α and β are always in the range of $\alpha = 0.7 \sim 1.0$, $\beta = 0.0 \sim 0.3$ [61]. Then, the value of F_σ^* is always in the range of $F_\sigma^* \approx 0.3$–0.6 [59].

For readers' convenience, the approximate formula can be provided as shown in Equation (7), which is created using the least-squares method. Equation (7) may provide F_σ^* for $\alpha = 0.7 \sim 1.0$, and $\beta = 0.0 \sim 0.3$ corresponding to all Resin/Metal combinations. Table 4 summarizes the exact values and Equation (7) values of F_σ^* in the range of $\alpha = 0.7 \sim 1.0, \beta = 0.0 \sim 0.3$ for metal and resin combination [59]. The values of Equation (7) are indicated in Fig. 10 for $\alpha = 0.7 \sim 1.0$, and $\beta = 0.0 \sim 0.3$ (metal/resin combination). As shown in Table 4 and Fig. 10, Equation (7) provides accurate values of F_σ^* within 1.3 % error.

$$\begin{aligned} F_\sigma^{*Eq.(7)} = &\left(-2.306 + 63.876\beta - 505.05\beta^2 + 1403.8\beta^3\right) \\ &+\left(10.325 - 217.85\beta + 1737.8\beta^2 - 4772\beta^3\right)\alpha \\ &+\left(-12.85 + 252.75\beta - 2000\beta^2 + 5425\beta^3\right)\alpha^2 \\ &+\left(5 - 97.777\beta + 766.65\beta^2 - 2055.5\beta^3\right)\alpha^3 \end{aligned} \tag{7}$$

Eq.(7) can be used for all Resin/Metal combination ($\alpha = 0.7 \sim 1.0, \beta = 0.0 \sim 0.3$) when $0 \leq h/W \leq 0.1$.

8. Adhesive geometry dependence of adhesive strength expressed as average stress prescribed in JIS

In this section, the variation of the average adhesive strength $\sigma_c^W(h)$ defined in Equation (1) will be derived on the numerical simulation. The discussion is based on the results that the adhesive strength can be expressed as a constant ISSF (For example, $K_{\sigma c} = 1.204\left[\text{MPa} \bullet \text{m}^{0.326}\right]$ for Resin B/S35C in Fig. 5). As shown in Fig. 9(b), the dimensionless ISSF $F_\sigma^*(h/W) = K_{\sigma c}/\left(\sigma_c^W(h)\, h^{1-\lambda}\right)$ in Equation (6a) becomes constant when $0 \leq h/W \leq 0.1$. Therefore, the constant value $C = K_{\sigma c}/F_\sigma^*(h/W)$ and the average adhesive strength $\sigma_c^W(h)$ can be obtained as shown in Equation (8).

$$\begin{aligned} &\sigma_c^W(h) = \frac{K_{\sigma c}}{F_\sigma^*}\frac{1}{h^{1-\lambda}} = \frac{C}{h^{1-\lambda}},\ C = \frac{K_{\sigma c}}{F_\sigma^*}\ (C: \text{Constant depending on } \alpha, \beta), \\ &\text{For Resin/Metal,} \\ &F_\sigma^* = F_\sigma^*(\alpha, \beta, h/W) \approx F_\sigma^*(\alpha, \beta) \approx 0.3 \sim 0.6 \text{ when } 0 \leq h/W \leq 0.1. \\ &K_{\sigma c} \approx 0.609 \sim 2.24 \text{MPa} \bullet \text{m}^{1-\lambda} \text{ (see Fig. 5)}, \\ &\lambda = 0.5946 \sim 0.9348 \text{ (see Ref[59])} \end{aligned} \tag{8}$$

The variation of the adhesive strength $\sigma_c^W(h)$ will be clarified when the adhesive geometrical dimension such as the adhesive area is larger

Table 2
Dimensionless ISSF F_σ^* of butt joint when $0 \le h/W \le 0.1$

	$\beta=-0.4$	$\beta=-0.3$	$\beta=-0.2$	$\beta=-0.1$	$\beta=0$	$\beta=0.1$	$\beta=0.2$	$\beta=0.3$	$\beta=0.4$
$\alpha=-1.0$	1.134	1.209	1.315	1.404	1.498				
$\alpha=-0.9$	1.066	1.148	1.252	1.347	1.424				
$\alpha=-0.8$	1.000	1.082	1.191	1.289	1.352				
$\alpha=-0.7$	0.904	1.032	1.134	1.223	1.288				
$\alpha=-0.6$		0.990	1.075	1.156	1.227	1.420			
$\alpha=-0.5$		0.946	1.028	1.119	1.185	1.360			
$\alpha=-0.4$		0.901	1.000	1.092	1.166	1.320			
$\alpha=-0.3$		0.812	0.940	1.057	1.142	1.280			
$\alpha=-0.2$		0.680	0.837	1.000	1.113	1.250	1.500		
$\alpha=-0.1$			0.710	0.916	1.061	1.230	1.460		
$\alpha=0$			0.585	0.799	1.000	1.195	1.430		
$\alpha=0.1$			0.460	0.654	0.873	1.124	1.380		
$\alpha=0.2$			0.353	0.550	0.758	1.000	1.314	1.918	
$\alpha=0.3$				0.456	0.643	0.858	1.181	1.769	
$\alpha=0.4$				0.384	0.558	0.740	1.000	1.572	
$\alpha=0.5$				0.326	0.476	0.630	0.813	1.293	
$\alpha=0.6$				0.257	0.405	0.546	0.686	1.000	
$\alpha=0.7$					0.340	0.470	0.588	0.794	1.730
$\alpha=0.8$					0.290	0.403	0.506	0.634	1.000
$\alpha=0.9$					0.223	0.333	0.430	0.543	0.746
$\alpha=1.0$					0.169	0.265	0.358	0.456	0.588[a]

[a] Misprint in Ref. [59] has been corrected.

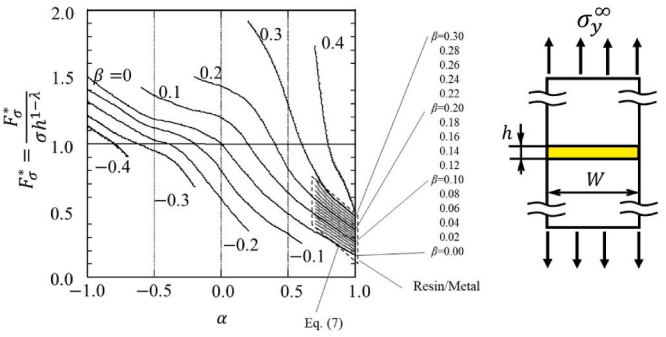

Fig. 10. Dimensionless F_σ^* under arbitrary material combination for $h/W \le 0.1$ for the entire range of Dundurs' parameters and values of Equation (7) for $\alpha = 0.70 \sim 1.0, \beta = 0.0 \sim 0.3$ (metal/resin combination).
$\alpha = \frac{G_1(\kappa_2+1)-G_2(\kappa_1+1)}{G_1(\kappa_2+1)+G_2(\kappa_1+1)}, \beta = \frac{G_1(\kappa_2-1)-G_2(\kappa_1-1)}{G_1(\kappa_2+1)+G_2(\kappa_1+1)}$, G_j: Shear modulus, $\kappa_j = 3-4\nu_j$ ($j = 1$(adherend), 2(adhesive))

than that of JIS ($A = W^2 > (12.7mm)^2$). The numerical solution based on Eq. (8) will be applied to the following cases. Case ①: The overall shape is constant and the size of the adhesive layer changes in the same way, Case ②: Only the thickness h of the adhesive layer changes, and Case ③: Only the specimen width W changes. Of these three cases, experiments have only been conducted for Case ②, and no experimental research has been conducted for Cases ① and ③. Therefore, in this study, the adhesive strength of these cases is examined by using numerical experiments based on the ISSF = constant conditions.

Fig. 11(a) illustrates the tensile adhesive strength of a prismatic butt joint when the shape ratio h/W of the adhesive layer is fixed and the overall dimensions of the adhesive layer are varied. In Fig. 11(a), the solid circle denotes the experimental result based on JIS σ_c^{JIS}. As shown in the results of $h/W = 0.1/12.7$ and $h/W = 0.5/10$ in Fig. 11(a), with a tenfold increase in the adhesive geometry, the adhesive strength decreases to 50 % of the JIS strength σ_c^{JIS}, and with a hundredfold increase, the adhesive strength decreases to 20 % of the JIS strength σ_c^{JIS}. In Fig. 11 (a), since the adhesive layer is similar, $F_\sigma^*(h/W)$ in Equation (6a) is constant. When the width W of the specimen and the thickness h of the adhesive layer change proportionally, the adhesive strength σ_c of the specimen can be expressed by Equation (9), which is illustrated in Fig. 11(a).

For Resin B/S35C

$$\sigma_c^W(h) = \frac{K_{\sigma c}}{\left[F_\sigma^*(h/W)h^{1-\lambda}\right]} = \frac{3.18}{h^{1-\lambda}}\,[\mathrm{MPa}] \tag{9a}$$

For $h/W = 0.1/12.7 \sim 1.0/12.7, F_\sigma^*(h/W) = 0.377$,

$K_{\sigma c} = 1.20\mathrm{MPa} \bullet m^{0.326}$

For Araldite/Aluminum

$$\sigma_c^W(h) = \frac{K_{\sigma c}}{\left[F_\sigma^*(h/W)h^{1-\lambda}\right]} = \frac{1.51}{h^{1-\lambda}}\,[\mathrm{MPa}]$$

For $h/W = 0.1/10 \sim 1.0/10, F_\sigma^*(h/W) = 0.403$,

$K_{\sigma c} = 0.609\mathrm{MPa} \bullet m^{0.286}$ (9b)

As shown in Fig. 9(b), since $F_\sigma^*(h/W)$ is insensitive to h/W, it can be used conveniently. From the practical adhesive layer thickness h in the range $h = 0.05 \sim 0.6mm$ and the practical adhesive area in $W \ge 12.7mm$, the relative adhesive thickness h/W is in the range $h/W \le 0.0472$. Therefore, for practical application of Resin B/S35C, $F_\sigma^*(0.1/12.7) \approx$ constant ≈ 0.377 and for practical application of Araldite/Aluminum, $F_\sigma^*(0.5/10) \approx$ constant ≈ 0.403, as shown in Fig. 9(b).

When the adhesive layer thickness is relatively large, i.e., when $h/W \cong 0.1$, there may be an error of about 5 % from the value of $F_\sigma^*(h/W) = const.$ depending on the material combination (see Fig. 9

Table 3
Dimensionless ISSF F_σ^* for actual material combination.

Adhesive	Young's modulus E^{Resin} [GPa]	Poisson's ratio ν^{Resin}	For Steel $E^{Steel} = 210$ GPa, $\nu^{Steel} = 0.3$		For Aluminum $E^{Al} = 70$ GPa, $\nu^{Al} = 0.3$	
			α, β	F_σ^*	α, β	F_σ^*
Weicon-Epoxy minute (Weicon, Germany) [62]	2.5	0.30	$\alpha = 0.976$ $\beta = 0.279$	0.451	$\alpha = 0.931$ $\beta = 0.266$	0.473
Araldite Standard-AS (Huntsman, Switzerland) [63]	1.8	0.38	$\alpha = 0.982$ $\beta = 0.189$	0.358	$\alpha = 0.947$ $\beta = 0.181$	0.375
Loctite-L3450 (Hexcel Composites, USA) [63]	1.8	0.38	$\alpha = 0.982$ $\beta = 0.189$	0.358	$\alpha = 0.947$ $\beta = 0.181$	0.375
Redux 326-Film (Hexcel Composites, USA) [64]	5.45	0.35	$\alpha = 0.946$ $\beta = 0.217$	0.410	$\alpha = 0.851$ $\beta = 0.192$	0.456
AS1805-RTV (Bridgwater, UK) [65]	0.0026	0.35	$\alpha = 0.999$ $\beta = 0.231$	0.385	$\alpha = 0.999$ $\beta = 0.231$	0.385
Sikaflex 552 (Sika, Portugal) [66]	0.0036	0.35	$\alpha = 0.999$ $\beta = 0.231$	0.385	$\alpha = 0.999$ $\beta = 0.230$	0.384
DP-8005 (3M Scotch-weld, USA) [67]	0.59	0.25	$\alpha = 0.995$ $\beta = 0.332$	0.489	$\alpha = 0.984$ $\beta = 0.328$	0.498
XNR6852E-2 (Nagase Chemtex, Japan) [67]	1.74	0.35	$\alpha = 0.983$ $\beta = 0.226$	0.392	$\alpha = 0.950$ $\beta = 0.218$	0.408
ESP 110 (Permabond, UK) [68]	4.6	0.35	$\alpha = 0.956$ $\beta = 0.219$	0.405	$\alpha = 0.872$ $\beta = 0.198$	0.446
Araldite-AV119 (Huntsman, UT) [68]	3.0	0.35	$\alpha = 0.971$ $\beta = 0.223$	0.398	$\alpha = 0.915$ $\beta = 0.209$	0.425
EC 3448 (3M Scotch-weld, USA) [68]	3.0	0.35	$\alpha = 0.971$ $\beta = 0.223$	0.398	$\alpha = 0.915$ $\beta = 0.209$	0.425
MY-753 (Huntsman, UT) [68]	1.88	0.35	$\alpha = 0.982$ $\beta = 0.226$	0.393	$\alpha = 0.946$ $\beta = 0.217$	0.410
Araldite 2015 (Huntsman, UT) [69]	1.85	0.33	$\alpha = 0.982$ $\beta = 0.249$	0.415	$\alpha = 0.947$ $\beta = 0.240$	0.433
Aralsite-AV138 (Huntsman, UT) [69]	4.89	0.35	$\alpha = 0.953$ $\beta = 0.219$	0.407	$\alpha = 0.865$ $\beta = 0.196$	0.450
Sika Force 7888 (Sika, Portugal) [69]	1.89	0.33	$\alpha = 0.982$ $\beta = 0.249$	0.415	$\alpha = 0.946$ $\beta = 0.239$	0.432
Araldite 2020 (Huntsman, UT) [70]	2.32	0.30	$\alpha = 0.978$ $\beta = 0.279$	0.449	$\alpha = 0.936$ $\beta = 0.267$	0.470
Araldite 2020 with 1 % cork (Huntsman, UT) [70]	2.14	0.30	$\alpha = 0.980$ $\beta = 0.280$	0.448	$\alpha = 0.941$ $\beta = 0.269$	0.468
FM 73M (Cytec Co.) [40]	4.2	0.45	$\alpha = 0.955$ $\beta = 0.083$	0.278	$\alpha = 0.872$ $\beta = 0.067$	0.318
Loctite 330 (Henkel, Germany) [71]	0.88	0.15	$\alpha = 0.992$ $\beta = 0.409$	0.585	$\alpha = 0.977$ $\beta = 0.404$	0.607

(b)). In such cases, the predicted tensile strength $\sigma_c^W(h)$ may also have an error of about 5 %. However, the adhesive strength of actual products sometimes varies about 10∼20 %, and the error in Equation (9) is within the error in the adhesive strength of actual product.

Next, Fig. 11(b) shows the adhesive strength by varying the adhesive layer thickness h under fixed W = constant. Note that the constant value of W does not affect the adhesive strength $\sigma_c^W(h)$. In other words, even if the adhesive area is different from JIS like $A = W^2 = (10mm)^2 \sim \infty$, the result of $F_\sigma^*(h/W)$ shows that the adhesive strength can be predicted from JIS specimen as $\sigma_c^W(h) = \sigma_c^{JIS}(h)$. For Resin B/steel, as shown in Fig. 11(b), the adhesive strength $\sigma_c^W(h)$ decreases with increasing the adhesive layer thickness h. The $\sigma_c^W(h) - h$ relation in Fig. 11(b) is corresponding to the $\sigma_c^W(h) - W$ in Fig. 11(a) when $h/W = 0.1/12.7 = 0.007874$.

For Araldite/Aluminum, as shown in Fig. 11(b), the adhesive strength $\sigma_c^W(h)$ decreases with increasing the adhesive layer thickness h. The $\sigma_c^W(h) - h$ relation in Fig. 11(b) is corresponding to the $\sigma_c^W(h) - W$ in Fig. 11(a) when $h/W = 0.5/10 = 0.05$. In this way, Equation (9) can be used to predict the adhesive strength $\sigma_c^W(h)$ for the adhesive geometry that has not actually been tested. For example, in the case of Araldite/Aluminum [33] , only experimental results were obtained for $h \geq 0.5mm$, but Equation (9) can be used to predict the adhesive strength $\sigma_c^W(h)$ for $h < 0.5mm$. For example, the adhesive strength $\sigma_c^W(h = 0.1mm)$ at $h = 0.1mm$ can be predicted as $\sigma_c^W(h = 0.1mm) = 20.8$ MPa.

Fig. 11(c) shows the adhesive strength by varying the specimen width W under fixed h = constant. As shown in previous studies [59], the adhesive strength is governed by the ISSF (denoted by $K_{\sigma c}$), i.e., $K_{\sigma c} = F_\sigma^*(h/W)\sigma_c h^{1-\lambda}$, so no matter how large the specimen width becomes, $\sigma_c^W(h)$ is constant as shown in Fig. 11(c). Therefore, if the adhesive layer thickness h is the same for the JIS specimen and the actual bonding, the same adhesive strength σ_c can be obtained regardless of the specimen width W. It may seem difficult to make the adhesive layer thickness of the actual adhesive h the same as the thickness of the specimen. However, this can be easily achieved by controlling the weight of adhesive applied per adhesive area (see Section 9).

Fig. 11(d) shows the adhesion strength $\sigma_c^W(h)$ by varying the adhesive area A in Cases ①∼③ shown in Fig. 11(a)–(c). Fig. 11(e) shows the adhesion strength $\sigma_c^W(h)$ by varying the volume V of the entire adhesive layer in Cases ①∼③ shown in Fig. 11(a)–(c). As shown in Fig. 11(d) and (e), even under the same A and even under the same V, the adhesive strength $\sigma_c^W(h)$ varies depending on h. As shown in Fig. 11 (e) when $h/W = 0.1/12.7$, and $h/W = 0.5/10$, with a tenfold increase in the adhesive geometry, the adhesive strength decreases to 50 % of the JIS strength σ_c^{JIS}, and with a hundredfold increase, the adhesive strength decreases to 20 % of the JIS strength σ_c^{JIS}. This is because the adhesive strength $\sigma_c^W(h)$ decreases with increasing the adhesive layer thickness h but independent of the specimen width W as mentioned above. Instead of the adhesive area A and the adhesive layer volume V which do not directly affect the adhesive strength $\sigma_c^W(h)$, the adhesive layer thickness

Table 4
Accuracy of Equation (7)
$F_\sigma^{*Eq.(7)}$ = Value of Eq. (7), F_σ^{*Exact} = Exact value of F_σ^*

	(a) $F_\sigma^{*Eq.(7)}/F_\sigma^{*Exact}$				(b) Value of Equation (7) $F_\sigma^{*Eq.(7)}$			
	$\beta = 0$	$\beta = 0.1$	$\beta = 0.2$	$\beta = 0.3$	$\beta = 0$	$\beta = 0.1$	$\beta = 0.2$	$\beta = 0.3$
$\alpha =$ 0.70	1.000	0.998	0.997	0.994	0.340	0.469	0.586	0.789
$\alpha =$ 0.80	1.000	0.998	0.996	0.992	0.290	0.402	0.504	0.629
$\alpha =$ 0.90	1.000	0.997	0.993	0.989	0.223	0.332	0.427	0.537
$\alpha =$ 1.00	1.000	0.996	0.992	0.987	0.169	0.264	0.355	0.450

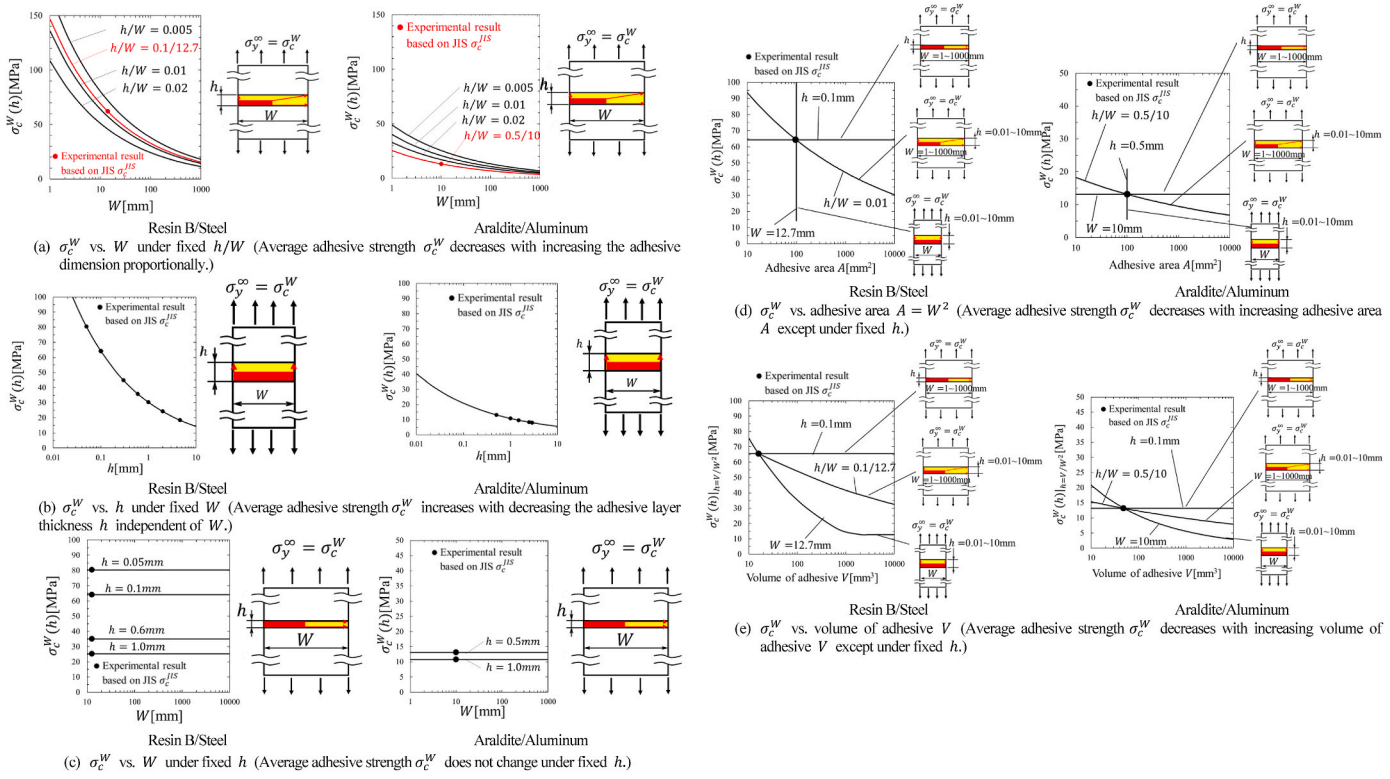

(a) σ_c^W vs. W under fixed h/W (Average adhesive strength σ_c^W decreases with increasing the adhesive dimension proportionally.)

(b) σ_c^W vs. h under fixed W (Average adhesive strength σ_c^W increases with decreasing the adhesive layer thickness h independent of W.)

(c) σ_c^W vs. W under fixed h (Average adhesive strength σ_c^W does not change under fixed h.)

(d) σ_c^W vs. adhesive area $A = W^2$ (Average adhesive strength σ_c^W decreases with increasing adhesive area A except under fixed h.)

(e) σ_c^W vs. volume of adhesive V (Average adhesive strength σ_c^W decreases with increasing volume of adhesive V except under fixed h.)

Fig. 11. Adhesive strength σ_c defined as an average stress $\sigma_c = P/A$ estimated from ISSF = const. In three models for Resin B/S35C. The solid circle denotes experimental results based on JIS σ_c^{JIS}.

h should be considered as the controlling factor of the adhesive strength $\sigma_c^W(h)$.

The results in Fig. 11 are based on the theory of elasticity with ISSF = constant assuming homogeneous adhesive without considering statistical factors such as numbers of defects in the adhesive layer. If the adhesive strength σ_c decreases experimentally with increasing the adhesive area or the volume of the adhesive layer under fixed adhesive layer thickness h, that is, even when the constant ISSF condition, the cause can be the increase of defects contained in the adhesive layer. Also, this study considers the strength under pure tension without considering bending stress, which may appear in adhesive structure having large adhesive areas.

9. Importance of controlling adhesive layer thickness

This study clarified that controlling the adhesive layer thickness h is essential for improving and evaluating the adhesive strength $\sigma_c^W(h)$. The reason can be summarized as follows.

1) The adhesive strength $\sigma_c^W(h)$ can be expressed as constant ISSF.
2) The ISSF $K_\sigma = F_\sigma^* \sigma_y^\infty h^{1-\lambda}$ is controlled by only the adhesive layer thickness h when the adhesive area $W^2 > (12.7mm)^2$.
3) The dimensionless ISSF $F_\sigma^* = K_\sigma/\sigma_y^\infty h^{1-\lambda}$ is constant for $h/W \leq 0.1$.

Therefore, the tensile test must be conducted with controlling the adhesive layer thickness h. One may think that controlling the adhesive layer thickness h is difficult, but the following method can be applied to make the adhesive layer thickness h in the JIS test specimen [39].

1) Fix two adherends on a jig with the adhesive surfaces of the two adherends spaced so that the thickness of the adhesive layer is h.
2) Attach cellophane tape to the bottom and both sides of the bonding area.
3) Drop the pre-vacuum defoamed adhesive into the upper part.
4) Place the adhesive in a vacuum desiccator, pull a vacuum, and inject the adhesive between the two adhesive surfaces.

When the adhesive layer thickness $h \leq 0.5$ mm is relatively small and the adhesive does not easily flow out from the end and side surfaces, a pair of adherends are placed on a precision electronic balance and the adhesive is applied to the adhesive surfaces of both adherends with a weight sufficient to obtain the specified h. This method is also relatively simple because the h is relatively small and the adhesive does not easily flow out from the end and side surfaces.

Once the JIS adhesive strength $\sigma_c^{JIS}(h = h_1)$ at a specific adhesive layer thickness $h = h_1$ is obtained, the adhesive strength can be expressed as shown in Equation (9) $\sigma_c^{JIS}(h) = C/h^{1-\lambda}$ (C: constant) as a function of h. The thickness h' of the adhesive in the actual product can be set relatively easily by controlling the weight of the adhesive applied per adhesive area. Then, the adhesive strength $\sigma_c^W(h)$ is obtained from $\sigma_c^W(h) = \sigma_c^{JIS}(h') = C/(h')^{1-\lambda}$ (C: constant). When the adhesive layer thickness h is well-controlled, even for much larger adhesive area than that of JIS specimens, the adhesive strength does not decrease very much. In other words, the adhesive strength $\sigma_c^{JIS}(h)$ in the JIS test specimen can be applied to much larger adhesive areas.

When the adhesive layer thickness h is not controlled, this study showed that the variation in adhesive strength varies by a factor of 5 depending on h. When the adhesive layer thickness h is controlled in the range of 0.05 mm $\leq h \leq$ 0.6 mm, which is commonly used in adhesive structures, the variation in adhesive strength is within a factor of 2. In order to discuss the strength of different adhesives, it is necessary to evaluate them under conditions of matched adhesive layer thicknesses.

One may think that even if the adhesive layer thickness h is well-controlled and even if the adhesive is carefully prepared by excluding air bubbles, the voids may appear in the adhesive layer resulting in reducing the adhesive strength [52]. However, the voids included inside of the adhesive do not affect the fracture very much since the stress concentration factor of the spherical void is around 2.045 [72] much smaller than the singular stress at the interface end. As indicated in the previous paper [52], the fracture originates from microcracks at or near the interface edge [52]. Therefore, if the edge of the interface is carefully prepared voids do not reduce the strength of the adhesive structures.

For readers' convenience, Fig. 12 illustrates the flowcharts to obtain the average strength $\sigma_c^W(h)$ for actual adhesive area $A = W^2 > (12.7mm)^2$. Two cases are considered: Fig. 12 (a) is the case where $\sigma_c^W(h)$ is obtained only from JIS experimental results and Fig. 12 (b) is the case where $\sigma_c^W(h)$ is obtained from experimental and analytical results confirming ISSF = constant. To calculate the ISSF, the flowchart provided in Fig. 12 with the explanation in Appendix A.

10. Conclusions

The Japanese Industrial Standards (JIS) specify the adhesive strength as an average ultimate tensile stress $\sigma_c^{JIS}(h) = P/A$, where $P =$ the maximum load, $A =$ the adhesive area, using a small specimen ($A = W^2 = (12.7mm)^2$) without considering the adhesive thickness h. On the other hand, several previous studies have shown that adhesive strength can be expressed as a constant ISSF. In this paper, therefore, after

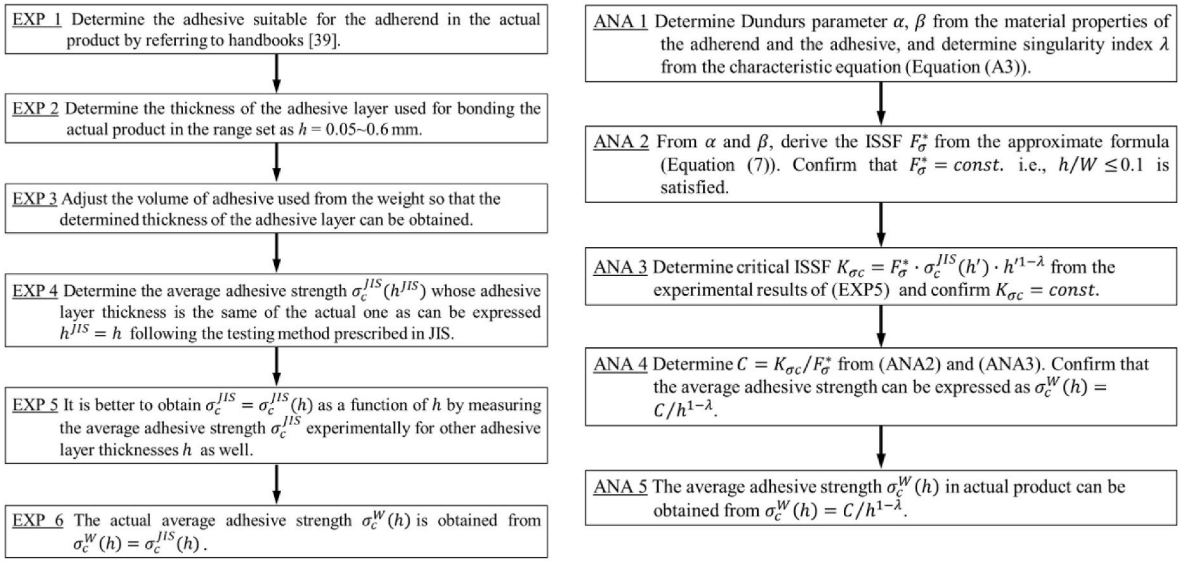

(a) To obtain the average adhesive strength $\sigma_c^W(h)$ of the actual product without analysis

(b) To obtain the actual average adhesive strength $\sigma_c^W(h)$ from analysis and experiment

Fig. 12. Flowchart to obtain the average adhesive strength $\sigma_c^W(h)$ of actual product.

confirming the validity of the ISSF, the dependence of adhesive strength $\sigma_c^W(h)$ on adhesive geometry was clarified when adhesive strength is expressed as the average stress. The conclusions can be summarized as follows:

(1) Care should be taken with the average adhesive strength σ_c^{JIS} defined in major standards such as JIS, ASTM, and ISO. For example, in butt joints, with a tenfold increase in the adhesive geometry, the adhesive strength decreases to 50 % of the JIS strength σ_c^{JIS}, and with a hundredfold increase, the adhesive strength decreases to 20 % of the JIS strength σ_c^{JIS} (see Fig. 11 (e) when $h/W = 0.1/12.7$ and $h/W = 0.5/10$).

(2) Care should be taken with the average adhesive strength σ_c^{JIS}, which varies significantly depending on adhesive layer thickness h. For example, σ_c^{JIS} varies as $\sigma_c^{JIS} = 76.8$–13.6 MPa when S35C is bonded with a common commercial adhesive Resin B. Even for the adhesive layer thickness $h = 0.05 \sim 0.6mm$ commonly used, it varies as $\sigma_c^{JIS} = 76.8$–35.7 MPa (see Fig. 2). The butt joint strength can be much larger than the bulk ductile adhesive strength as $\sigma_c = (1.715 \sim 0.781)\sigma_B^{Bulk}$ for Resin B/S35C, $\sigma_B^{Bulk} = 46.8$ MPa (see Fig. 2).

(3) Even when the adhesive area is much larger in actual products than that of the JIS specimen as $A = W^2 \gg (12.7mm)^2$, the JIS tensile adhesive strength $\sigma_c^{JIS}(h)$ can be applied as $\sigma_c^W(h) = \sigma_c^{JIS}(h)$, provided that the adhesive layer thickness h is the same in the actual products and the JIS (see Fig. 11(c)).

(4) The reason why the average adhesive strength $\sigma_c^{JIS}(h) = P/A$ can be applied to much larger adhesive areas can be explained as follows. The dimensionless ISSF $F_\sigma^* = K_\sigma/\sigma h^{1-\lambda} \approx$ constant can be regarded as a constant value within an error of 3.5 % in the range $h/W \leq 0.1$, independent of adhesive areas. In other words, the ISSF F_σ^* only depends on the adhesive layer thickness h, independent of other geometries (see Fig. 9(b)).

(5) For JIS specimens, the adhesive layer thickness h can be made constant easily by placing a pair of adherends on a precision electronic balance and applying enough weight of adhesive to the adhesive surfaces of both adherends to obtain the specified h. The adhesive layer thickness in actual products can be determined relatively easily by controlling the weight of adhesive applied per adhesive area.

(6) When the adhesive layer thickness h is controlled well, even for much larger adhesive area than those of JIS specimens, the adhesive strength does not decrease significantly. In other words, the adhesive strength $\sigma_c^{JIS}(h)$ in the JIS test specimen can be applied to much larger adhesive areas.

CRediT authorship contribution statement

Nao-Aki Noda: Writing – review & editing, Writing – original draft, Validation, Supervision, Investigation, Conceptualization. **Rei Takaki:** Writing – review & editing, Writing – original draft, Visualization, Validation, Investigation, Formal analysis. **Yasuaki Suzuki:** Validation, Investigation. **Yasushi Takase:** Visualization, Formal analysis. **Kazuhiro Oda:** Validation, Supervision, Investigation.

Declaration of competing interest

The authors declare the following financial interests/personal relationships which may be considered as potential competing interests: Rei Takaki reports financial support was provided by Public Interest Incorporated Foundation Research Foundation for the Electrotechnology of Chubu (Grant ID : R-04111). If there are other authors, they declare that they have no known competing financial interests or personal relationships that could have appeared to influence the work reported in this paper.

Appendix A. Mesh independent proportional method to calculate ISSF

In this Appendix A, the outline of the proportional method originally proposed will be explained to analyze the ISSF. Figure A1(a) illustrates a butt joint when $h/W = 0.001$ and Figure A1(b) illustrates a bonded plate corresponding to the butt joint in Fig. 1(a) when $h/W \geq 1$. As shown in Figure A1 (a), (b), singular stress fields are illustrated as shown in Equation (A1).

$$\sigma_y^{real}(r) \to \frac{K_\sigma}{r^{1-\lambda}} \ (r \to 0) \text{ in Figure A1} \tag{A1}$$

When the bad pair condition $\alpha(\alpha - 2\beta) > 0$ is satisfied, the interface stress has singularity in Equation (A1). Here, α, β are Dundurs' parameters defined in Eq. (A2) [41,42].

$$\alpha = \frac{G_1(\kappa_2+1) - G_2(\kappa_1+1)}{G_1(\kappa_2+1) + G_2(\kappa_1+1)}, \beta = \frac{G_1(\kappa_2-1) - G_2(\kappa_1-1)}{G_1(\kappa_2+1) + G_2(\kappa_1+1)},$$
$$\kappa_j = \begin{cases} \dfrac{3-\nu_j}{1+\nu_j} \text{ (plane stress)} \\ 3 - 4\nu_j \text{ (plane strain)} \end{cases}, j = 1(\text{adherend}), 2(\text{adhesive}) \tag{A2}$$

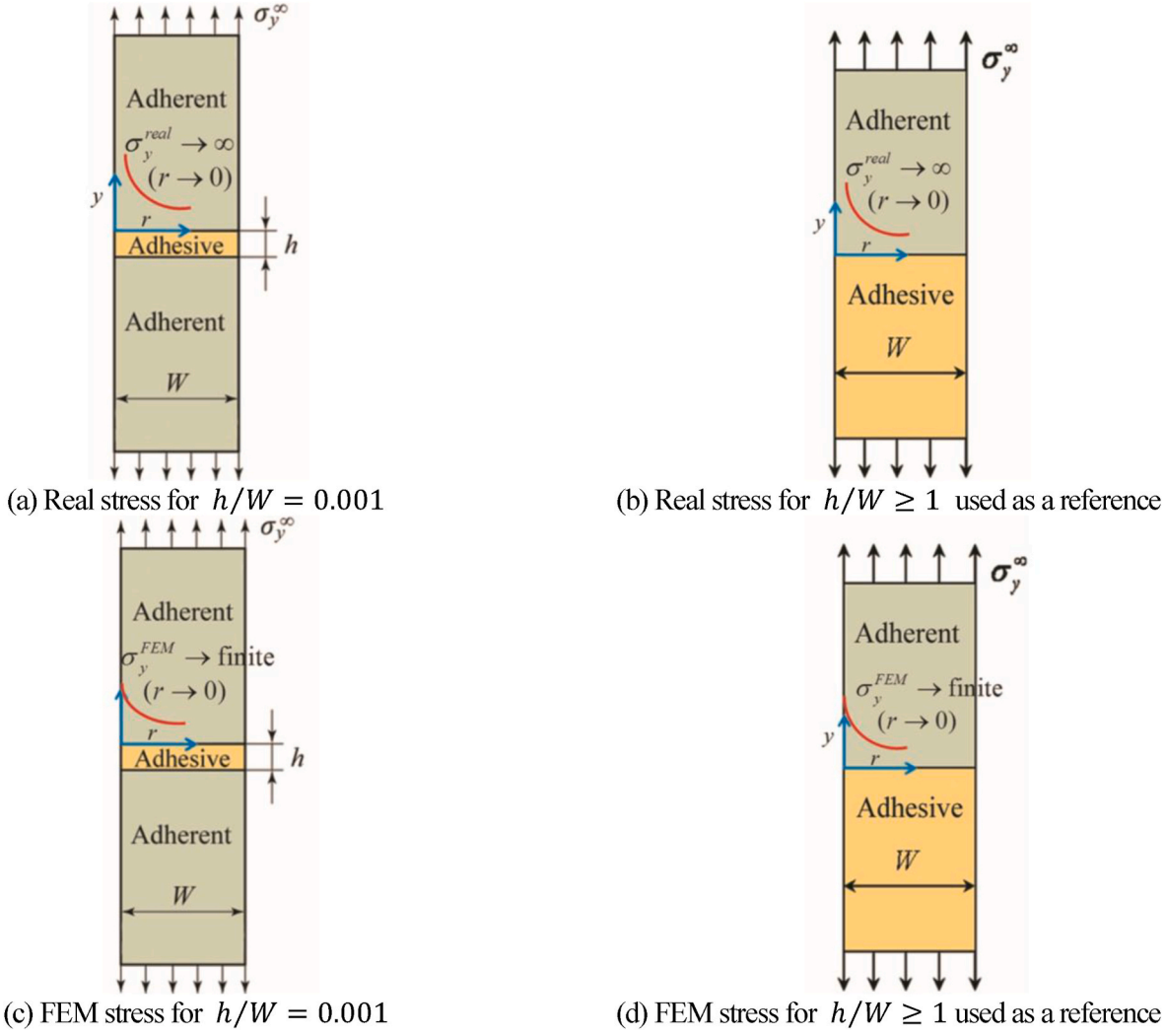

Fig. A1. Real stress for (a) $h/W = 0.001$, (b) $h/W \geq 1$ and FEM stress for (c) $h/W = 0.001$, (d) $h/W \geq 1$

The value of the singularity index λ in Equation (A2) can be determined as the minimum root in Eq. (A3), which can be derived from the boundary condition around the interface end $r = 0$ in Figure A1.

$$\left[sin^2\left(\frac{\pi}{2}\lambda\right) - \lambda^2\right]^2\beta^2 + 2\lambda^2\left[sin^2\left(\frac{\pi}{2}\lambda\right) - \lambda^2\right]\alpha\beta + \lambda^2\left(\lambda^2 - 1\right)\alpha^2 + \frac{sin^2(\pi\lambda)}{4} = 0 \tag{A3}$$

When $\alpha(\alpha - 2\beta) > 0$ is satisfied, Equation (A3) has a single and real root in the range $0 \leq \lambda \leq 1$ and the singular stress field in Equation (A1) is formed. Then, the ISSF K_σ in Figure A1 (a), (b) is defined as Equation (A4).

$$K_\sigma = \lim_{r \to 0}\left[r^{1-\lambda} \times \sigma_y^{real}(r)\right] \tag{A4}$$

The dimensionless ISSF F_σ is defined as [48]

$$F_\sigma = \frac{K_\sigma}{\sigma_y^\infty W^{1-\lambda}} \tag{A5}$$

The real stress distributions $\sigma_y^{real}(r)$ in Figure A1(a), (b) are proportional and they go to infinity as $\sigma_y^{real}(r) \to \infty (r \to 0)$. Instead, FEM stress distributions in Figure A1(c), (d) are finite as $\sigma_y^{FEM}(r) \to finite\ (r \to 0)$ and the value $\sigma_y^{FEM}(r)$ at $r \approx 0$ varies depending on of FEM mesh size. Here, $\sigma_y^{FEM}(r)$ denotes FEM stress obtained by the finite element method. Although FEM stress distributions $\sigma_y^{FEM}(r)$ cannot be singular, but they can be proportional if the same FEM mesh pattern is applied.

Table A1 shows the FEM stress $\sigma_y^{FEM}(r)$ obtained by the FEM for (a) $h/W = 0.001$ and (b) $h/W \geq 1$. Since the exact solution [48] is available for $h/W \geq 1$, Figure A1(b), (d) can be used as a reference problem. In Table A1, the value of $\sigma_y^{FEM}(r)$ varies depending on the FEM mesh size due to the singularity of the real stress $\sigma_y^{real}(r)$.

$$K_\sigma \neq \lim_{r \to 0}\left[r^{1-\lambda} \times \sigma_y^{FEM}(r)\right] \tag{A6}$$

In Table A1, the FEM stress ratio $\sigma_y^{FEM}/\sigma_{y(Ref)}^{FEM}$ is also shown. It is seen that the FEM stress ratio $\sigma_y^{FEM}/\sigma_{y(Ref)}^{FEM}$ is independent of the mesh size. This is because the FEM error is controlled by the mesh size around $r = 0$. Table A1 shows that the FEM stress distributions are also proportional when the same FEM mesh pattern is applied.

As shown in Eq. (A6), the ratio of ISSF $K_\sigma/K_{\sigma(Ref)}$ is controlled by the ratio of stress $\lim_{r\to 0}\left[\sigma_y(r)/\sigma_{y(Ref)}(r)\right]$. Here, the subscript (Ref) denotes the reference problem.

$$\frac{K_\sigma}{K_{\sigma(Ref)}} = \lim_{r\to 0}\frac{\left[r^{1-\lambda}\times\sigma_y^{real}(r)\right]}{\left[r^{1-\lambda}\times\sigma_{y(Ref)}^{real}(r)\right]} = \lim_{r\to 0}\frac{\left[r^{1-\lambda}\times\sigma_y^{FEM}(r)\right]}{\left[r^{1-\lambda}\times\sigma_{y(Ref)}^{FEM}(r)\right]}$$
$$\text{but } \lim_{r\to 0}\left[r^{1-\lambda}\times\sigma_y^{real}(r)\right] \neq \lim_{r\to 0}\left[r^{1-\lambda}\times\sigma_y^{FEM}(r)\right] \tag{A7}$$
$$\frac{K_\sigma}{K_{\sigma(Ref)}} = \frac{F_\sigma\sigma_y^\infty W^{1-\lambda}}{F_{\sigma(Ref)}\sigma_{y(Ref)}^\infty W^{1-\lambda}} = \frac{F_\sigma}{F_{\sigma(Ref)}}$$

To obtain the ISSF K_σ from the ratio $K_\sigma/K_{\sigma(Ref)}$, the reference solution $F_{\sigma(Ref)}$ in Figure A1 can be used conveniently because the exact ISSF has been investigated under arbitrary material combination. This proportional method described in Appendix A can be used conveniently to analyze the ISSF.

Table A1
Stress distributions for bonded strip under tension shown in Figure A1 obtained by different mesh size when $h/W = 0.001$

Smallest mesh size $e_{min} = 1/3^8$ around the edge			Smallest mesh size $e_{min} = 1/3^4$ around the edge		
r/W	$\sigma_y^{FEM}\|_{h/W=0.001}$	$\frac{\sigma_y^{FEM}\|_{h/W=0.001}}{\sigma_{y(Ref)}^{FEM}}$	r/W	$\sigma_y^{FEM}\|_{h/W=0.001}$	$\frac{\sigma_y^{FEM}\|_{h/W=0.001}}{\sigma_{y(Ref)}^{FEM}}$
	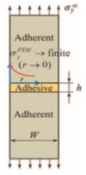	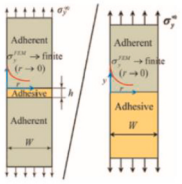		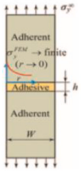	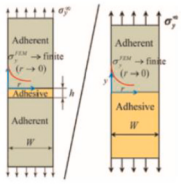
0/3^8	1.414	0.525	0/3^4	1.072	0.524
1/3^8	1.177	0.525	1/3^4	0.889	0.522
2/3^8	1.138	0.525	2/3^4	0.859	0.522
3/3^8	1.109	0.525	3/3^4	0.838	0.522
4/3^8	1.088	0.525	4/3^4	0.824	0.523
5/3^8	1.071	0.525	5/3^4	0.813	0.525

Table A2 and Figure A2 show the exact value of $F_\sigma(h/W) = K_\sigma/\left(\sigma W^{1-\lambda}\right)$ of the bonded plate for the whole range of Dundurs' parameter α, β [73]. The dimensionless function of θ was clarified by Carpenter and Byers [74]. The bonded plate in Figure. A2 can be regarded as a plate butt joint with a very thick adhesive layer for $h/W \geq 1$. The exact values of F_σ were obtained by the body force method under the bad pair condition of $\alpha(\alpha - 2\beta) > 0$ [48,59,75] and they were obtained by FEM under the good pair and equal pair conditions of $\alpha(\alpha - 2\beta) \leq 0$. Since the solution for thin adhesive layer $h/W \leq 0.1$ is indicated in Fig. 10 under arbitrary material combination, the accurate results can be obtained by the interpolation also in the range $0.01 \leq h/W \leq 1.0$. However, the expression $F_\sigma^*(h/W) = K_\sigma/\left(\sigma h^{1-\lambda}\right)$ in Equation (6a) for Resin/Metal and Table A2 and Fig. 10 indicated under arbitrary material combination indicated in Section 7 are useful in the range $0 \leq h/W \leq 0.1$ and therefore enough for practical applications.

Table A2
$F_\sigma|_{h/W=1}$ at interface edge point in bonded finite plate

	$\beta = -0.4$	$\beta = -0.3$	$\beta = -0.2$	$\beta = -0.1$	$\beta = 0$	$\beta = 0.1$	$\beta = 0.2$	$\beta = 0.3$	$\beta = 0.4$
$\alpha = -1.0$	0.540	0.446	0.395	0.357	0.332				
$\alpha = -0.95$	0.643	0.491	0.422	0.381	0.349				
$\alpha = -0.9$	0.726	0.534	0.456	0.412	0.381				
$\alpha = -0.8$	1.000	0.636	0.538	0.487	0.450				
$\alpha = -0.7$	1.855	0.800	0.626	0.558	0.486				
$\alpha = -0.6$	3.291	1.000	0.724	0.638	0.559	0.505			
$\alpha = -0.5$		1.264	0.842	0.722	0.635	0.551			
$\alpha = -0.4$		1.467	1.000	0.822	0.718	0.615			
$\alpha = -0.3$		1.609	1.118	0.913	0.796	0.697			
$\alpha = -0.2$		1.690	1.153	1.000	0.889	0.797	0.404		

(continued on next page)

Table A2 (*continued*)

	$\beta = -0.4$	$\beta = -0.3$	$\beta = -0.2$	$\beta = -0.1$	$\beta = 0$	$\beta = 0.1$	$\beta = 0.2$	$\beta = 0.3$	$\beta = 0.4$
$\alpha = -0.1$			1.103	1.037	0.955	0.890	0.767		
$\alpha = 0$			1.000	1.000	1.000	1.000	1.000		
$\alpha = 0.1$			0.767	0.890	0.955	1.037	1.103		
$\alpha = 0.2$			0.404	0.797	0.889	1.000	1.153	1.690	
$\alpha = 0.3$				0.697	0.796	0.913	1.118	1.609	
$\alpha = 0.4$				0.615	0.718	0.822	1.000	1.467	
$\alpha = 0.5$				0.551	0.635	0.722	0.842	1.264	
$\alpha = 0.6$				0.505	0.559	0.638	0.724	1.000	3.291
$\alpha = 0.7$					0.486	0.558	0.626	0.800	1.855
$\alpha = 0.8$					0.450	0.487	0.538	0.636	1.000
$\alpha = 0.9$					0.381	0.412	0.456	0.534	0.726
$\alpha = 0.95$					0.349	0.381	0.422	0.491	0.643
$\alpha = 1.0$					0.332	0.357	0.395	0.446	0.540

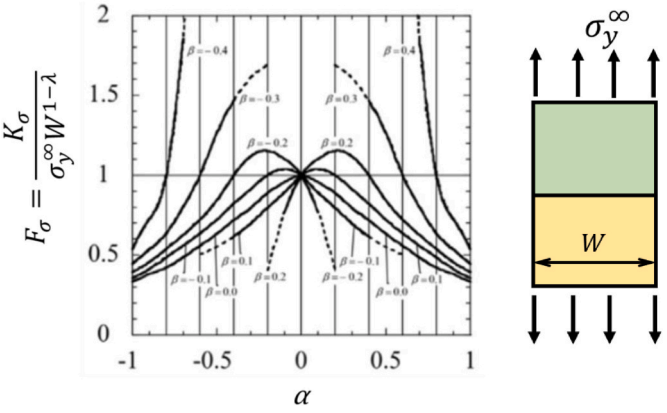

Fig. A2. ISSF for the bonded plate useful for $h/W \geq 1.0$

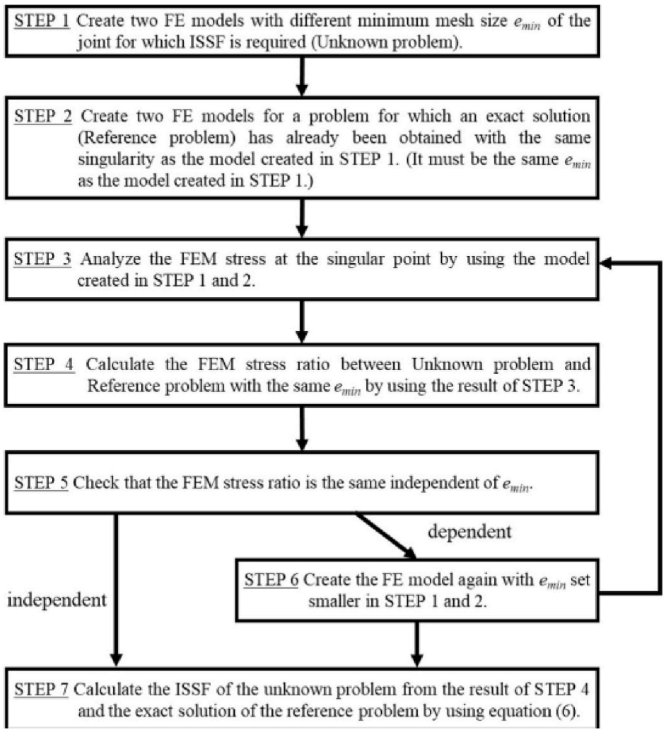

Fig. A3. Flowchart for applying the mesh-independent proportional method to calculate the ISSF.

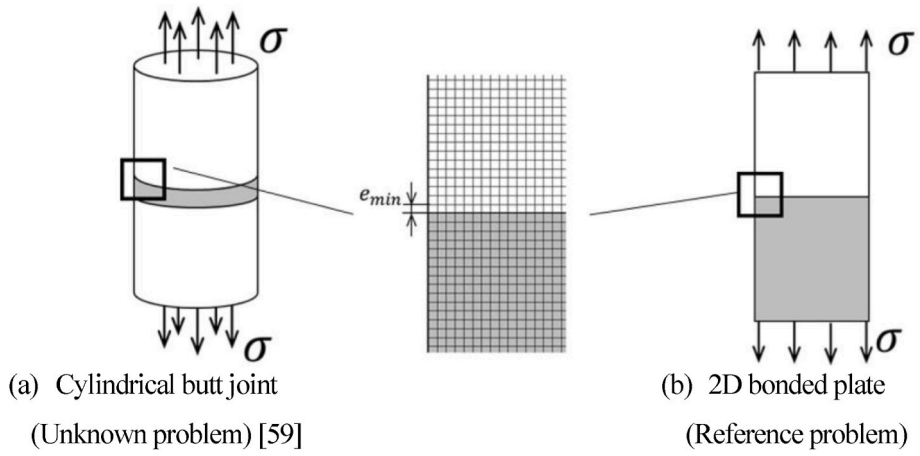

Fig. A4. Example of analysis model and mesh pattern.

Figure A3 illustrates the flowchart to calculate the ISSF in 3D bonded geometries by applying the proportional method. 2D modelling is often useful although validity confirmation is desirable. The flowchart in Figure A3 indicates elementary step-by-step actions by applying the proportional method to calculate ISSFs. Here, a cylindrical butt joint in Figure A4 [58] is assumed as an example of an unknown problem.

First of all, as STEP 1, two kinds of minimum FE mesh size e_{min} are applied to the cylindrical butt joint (=unknown problem). Next, as STEP 2, those two kinds of minimum FE mesh size e_{min} are applied to the bonded plate (=reference problem) whose exact solution is available [75]. Note that the reference problem and the unknown problem have the same singular stress field but different ISSF. As STEP 3, the FEM stresses at the singular points are calculated for the unknown and the reference problems by applying FEM. As STEP 4, the FEM stress ratio of the unknown and reference problems is obtained. This is because the FEM stress around the singular point is not the real stress and depends on the FEM mesh size. As STEP 5, the mesh-independency of the stress ratio is investigated. Since the same FEM mesh is applied around the singular point, the FEM error can be eliminated. STEP 6 is required when two ratios are not the same. Instead, if two ratios are the same, as STEP 7, the FEM stress ratio can be used as the ISSF ratio. Then, the ISSF of the unknown problem can be provided from the ISSF ratio and the exact ISSF of the reference problem. In the case of STEP 6, since the previous mesh sizes are not appropriate, the new FE models are newly created using smaller mesh size and go to STEP3.

In this Appendix A, the mesh-independent proportional method was explained by taking examples of the 2D butt joint in Fig. A1 and the axisymmetric cylindrical butt joint problem in Figure A4. Recently, Miyazaki et al. [12,13] analyzed the ISSF as well as the singularity index (SI) at the interface corner of three dimensional (3D) prismatic bonded joints. In these studies, the relation between the minimum mesh size e_{min} and the FEM stresses $\sigma_{FEM}(r)$ under this mesh e_{min} were investigated by varying the size $e_{\min}$ around the corner point. Then, mesh-independent formulas such as $\sigma_{FEM}(r)\cdot(e_{min})^{1-\lambda} = \text{const.}$ and other useful expressions for ISSFs were theoretically derived on the basis of the proportional stress fields in several prismatic butt joints having similar FEM mesh pattern. This mesh-independent proportional method can be used for analyzing corner ISSFs in general 3D dissimilar problems efficiently.

Data availability

Data will be made available on request.

References

[1] Journal of Society of Automotive Engineers of Japan. Special feature, Dissimilar material joining technologies and multi-material structures of vehicle 2023;77(7).
[2] Noda NA. ISSF method to evaluate adhesive strength for metal and resin. J Soc Automot Eng Jpn 2023;77(7):30–9.
[3] Rachid HB, Noureddine D, Benali B, Adin MS. Effect of nanocomposites rate on the crack propagation in the adhesive of single lap joint subjected to tension. Mech Adv Mater Struct 2024;31(25):6898–906.
[4] Hamit Adin ST, Sulu IY. Behaviour of bi-adhesive in double-strap joiint with embedded patch subjected to bending. J Theor Appl Mech 2015;45(3):83–96.
[5] Galvez P, Noda NA, Takaki R, Sano Y, Miyazaki T, Abenojar J, Martínez MA. Intensity of singular stress field (ISSF) variation as a function of the Young's modulus in single lap adhesive joints. Int J Adhesion Adhes 2019;95:102418.
[6] Puspaningtyas CP, Jusuf A, Hadi BK, Yudhanto A. Modeling of single-lap joints with auxetic adhesive utilizing homogeneous and heterogeneous bondline microstructures. Heliyon 2024;10:e24141.
[7] Houjou K, Shimamoto K, Akiyama H, Sato C. Effect of test temperature on the shear and fatigue strengths of epoxy adhesive joints. J Adhes 2022;98:2599–617.
[8] Houjou K, Shimamoto K, Akiyama H, Terasaki N, Sato C. Calculation of the moisture diffusion coefficient at the adhesive interface of double cantilever beam specimens by studying the fracture surfaces. Polym Test 2023;125:108141.
[9] Houjou K, Akiyama H, Sato C. Fatigue fracture behavior of cured epoxy adhesive containing a surface crack. Polym Test 2023;117:107821.
[10] Noda NA, Takaki R. Adhesive strength improvement by providing steps in joints and differenting initial and final debonding stresses. Mater Des 2024;245:113258.
[11] Oda K, Oda H, Takase Y, Noda NA. Strength analysis due to thermal loading and tensile loading when metals are bonded by heat-curing adhesives. Therm Sci Eng Prog 2024;55:102967.
[12] Miyazaki T, Fukuda H, Noda NA. Mesh-independent proportional method to obtain ISSF and singularity index at the interface corner of three-dimensional dissimilar structures. Eng Fract Mech 2025;314:110624.
[13] Miyazaki T, Fujiwara T, Noda NA, Sano Y. Three-dimensional singularity index at interface corner in prismatic butt joint under arbitrary material combination. Int J Solid Struct 2021;229(15):111120.
[14] Miyazaki T, Noda NA, Ren F, Wang Z, Sano Y, Iida K. Analysis of intensity of singular stress field for bonded cylinder and bonded pipe in comparison with bonded plate. Int J Adhesion Adhes 2017;77:118–37.
[15] Bendemra H, Compston P, Crothers PJ. Optimization study of tapered scarf and stepped-lap joints in composite repair patches. Compos Struct 2015;130:1–8.
[16] Katnam KB, Da Silva LFM, Young TM. Bonded repair of composite aircraft structures: a review of scientific challenges and opportunities. Prog Aero Sci 2013;61:26–42.
[17] Goede M, Stehlin M, Rafflenbeul L, Kopp G, Beeh E. Super Light Car -lightweight construction thanks to a multi-material design and function integration. European Transport Research Review 2009;1:5–10.
[18] Watson B, Nandwani Y, Worswick MJ, Cronin DS. Metallic multi-material adhesive joint testing and modeling for vehicle lightweighting. Int J Adhesion Adhes 2019;95:102421.
[19] Naito J, Suzuki R. Multi-material automotive bodies and dissimilar joining technology to realize multi-material. Kobelco Technol Rev 2020;38:32–7.
[20] Blanco D, Rubio EM, Marín MM, Davim JP. Advanced materials and multi-materials applied in aeronautical and automotive fields: a systematic review approach. Procedia CIRP 2021;99:196–201.
[21] Beber VC, Brede M. Multiaxial static and fatigue behaviour of elastic and structural adhesives for railway applications. Procedia Struct Integr 2020;28:1950–62.
[22] Liu Y, Carnegie C, Ascroft H, Li W, Han X, Guo H, Hughes DJ. Investigation of adhesive joining strategies for the application of a multi-material light rail vehicle. Material 2021;14(22):6991.

[23] Delzendehrooy F, Akhavan-Safar A, Barbosa AQ, Beygi R, Cardoso D, Carbas RJC, Marques EAS, da Silva LFM. A comprehensive review on structural joining techniques in the marine industry. Compos Struct 2022;289(1):115490.
[24] Barnes TA, Pashby IR. Joining techniques for aluminium spaceframes used in automobiles: Part II - adhesive bonding and mechanical fasteners. J Mater Process Technol 2000;99(1–3):72–9.
[25] Tserpes K, Barroso-Caro A, Carraro PA, Beber VC, Floros I, Gamon W, Kozłowski M, Santandrea F, Shahverdi M, Skejić D, Bedon C, Rajčić V. A review on failure theories and simulation models for adhesive joints. J Adhes 2021;98(12):1855–915.
[26] Ramalho LDC, Campilho RDSG, Belinha J, da Silva LFM. Static strength prediction of adhesive joints: a review. Int J Adhesion Adhes 2020;96:102451.
[27] Mori K, Isono H, Sugibayashi T. Fracture behavior and strength of stepped-lap bonded joint with adhesive resin under tensile loading. Transaction of The Japan Society of Mechanical Engineers Series A 1994;60(569):71–9.
[28] Mori K, Sugibayashi T. Effect of number of steps on stress distribution and final fracture strength of stepped-lap bonded joint, Transaction of Japan Society of Mechanical Engineers Series A 1989;55(519):2211–9.
[29] Japan Industrial Standard. JISK6848 Adhesives−Testing methods of bonding strength of adhesives 1999.
[30] Japan Industrial Standard. JIS K6849 Testing methods for tensile strength of adhesive bonds 1994.
[31] ISO6922. Adhesive- Determination of tensile strength of butt joints 1987.
[32] Suzuki Y. Adhesive tensile strengths of scarf and butt joints of steel plates (3rd report, relation between adhesive layer thicknesses and adhesive strengths of joints). JSME International Journal 1987;30(No.265):1042–51.
[33] Akisanya AR, Meng CS. Initiation of fracture at the interface corner of bi-material joints. Journal of Mechanical Physics and Solids 2003;51(1):27–46.
[34] Reedy Jr ED, Guess TR. Interface corner failure analysis of joint strength: effect of adherend stiffness. Int J Fract 1997;88:305–14.
[35] ASTM D5656. Standard test method for thick-adherend metal lap-shear joints for determination of the stress-strain behavior of adhesives in shear by tension loading 2005.
[36] The Adhesion Society of Japan. Adhesion handbook. fourth ed. Nikkan Kogyo Shinbun, Ltd.; 2007.
[37] The Adhesion Society of Japan. Adhesion technique textbook for aspiring professionals. Nikkan Kogyo Shinbun, Ltd.; 2009.
[38] Ono M. JIS usage series: adhesion and adhesives - how to select and use them. New Edition. Japanese Standards Association; 1989.
[39] Suzuki Y. Adhesion Engineering -Bonding and joining of dissimilar materials, improvement of strength, reliability and durability. Life prediction methods-. Maruzen Publishing; 2018.
[40] Park JH, Choi JH, Kweon JH. Evaluating the strengths of thick aluminum-to-aluminum joints with different adhesive lengths and thicknesses. Compos Struct 2010;92:2226–35.
[41] Bogy DB. Edge-bonded dissimilar orthogonal elastic wedges under normal and shear loading. Transactions of the ASME Journal of Applied Mechanics 1968;35(3):460–6.
[42] Bogy DB. Two edge-bonded elastic wedges of different materials and wedge angles under surface tractions. Transactions of the ASME Journal of Applied of Mechanics 1971;38(No.2):377–86.
[43] Hein VL, Erdogan F. Stress singularities in a two-material wedge. Int J Fract 1971;7:317–30.
[44] Chen DH, Nisitani H. Singular stress field near the corner of jointed dissimilar materials. Transactions of the ASME Journal of Applied Mechanics 1993;60(3):607–13.
[45] Shibutani T. Evaluation of crack initiation at interfacial edge on the basis of fracture mechanics concept and application to electronics devices. Journal of The Japan Institute of Electronics Packaging 2004;7(7):639–44.
[46] Shiratori M. Problems of joints in packaging of electronic devices. Trans JSME Series A 1994;60(577):1905–12.
[47] Hattori T, Sakata S, Hatsuta T, Murakami H. A stress singular parameters approach for evaluating adhesive strength. Trans JSME Series A 1988;54(499):597–603.
[48] Noda NA, Miyazaki T, Li R, Uchikoba T, Sano Y, Takase Y. Debonding strength evaluation in terms of the intensity of singular stress at the interface corner with and without fictitious crack. Int J Adhesion Adhes 2015;61:46–64.
[49] Noda NA, Takaki R, Sano Y, Wang B. ISSF method to evaluate adhesive strength when two distinct singular stress field appear along the interface. Int J Fract 2023;241:95–114.
[50] Li R, Noda NA, Takaki R, Sano Y, Takase Y, Miyazaki T. Most suitable evaluation method for adhesive strength to minimize bend effect in lap joints in terms of the intensity of singular stress field. Int J Adhesion Adhes 2018;86:45–58.
[51] Takaki R, Noda NA, Ren F, Sano Y, Takase Y, Miyazaki T, Suzuki Y, Lan X. Variation of intensity of singular stress field (ISSF) along the interface outer edge of prismatic butt joint and debonding condition expressed by the ISSF. Int J Adhesion Adhes 2020;102:102665.
[52] Takaki R, Noda NA, Sano Y, Takase Y, Suzuki Y, Chao CK. Fractographic identification of fracture origin mainly controlled by the intensity of singular stress field (ISSF) in prismatic butt joint with corner fillet. Int J Adhesion Adhes 2021;106:102810.
[53] Marc Mentat Team. Theory and user information, A. Tokyo: MSC, Software; 2019.
[54] Miyazaki T, Inoue T, Noda NA, Sano Y. A precise and efficient method for evaluating singular stress field at the vertex in three-dimensional bonded body. Trans JSME Series A 2018;84(864).
[55] Harada S, Noda NA, Fukasako I, Endo T. Effects of notch sharpness and plate thickness on the fracture toughness K_{Ic} of acrylic resin. Journal of The Society of Materals Science Japan 1986;35(397):1157–62.
[56] Suzuki Y. Adhesive tensile strengths of scarf and butt joints of steel plates (2nd report, relation between mechanical properties of adhesives and fracture criteria of joints). Bulletin of JSME 1985;28(No.245):2575–84.
[57] Koguchi H, Attaporn W. Analysis of Elasto−Plastic stress singularity around interface free edge in joints using FEM. Proceedings of The Society of Materials Science Japan 2006;55:259–60.
[58] Suzuki Y. Stress analysis and strength of adhesive lap joints loaded in tension. JSME Proceedings 1990;900–86:395–7.
[59] Noda NA, Ren F, Takaki R, Wang Z, Oda K, Miyazaki T, Sano Y. Intensity of singular stress field over the entire bond line thickness range useful for evaluating the adhesive strength for plate and cylinder butt joints. Int J Adhesion Adhes 2018;85:234–50.
[60] Akhavan-Safar A, da Silva LFM, Ayatollahi MR. An investigation on the strength of single lap adhesive joints with a wide range of materials and dimensions using a critical distance approach. Int J Adhesion Adhes 2017;78:248–55.
[61] Noda NA, Oda K, Takase Y, Hotta G. Fracture mechanics for the design of bonded dissimilar materials and structures, Corona publishing co. ltd.; 2023.
[62] Ayatollahi MR, Akhavan-Safar A. Failure load prediction of single lap adhesive joints based on a new linear elastic criterion. Theor Appl Fract Mech 2015;80:210–7.
[63] Morais AB, Pereira AB, Teixeira JP, Cavaleiro NC. Strength of epoxy adhesive bonded stainless steel joints. Int J Adhesion Adhes 2007;27:679–86.
[64] Da Silva LF, Adams R, Gibbs M. Manufacture of adhesive joints and bulk specimens with high-temperature adhesives. International Journal of Adhesion and Adhesives 2004;24:69–83.
[65] Banea MD, da Silva LF. Static and fatigue behaviour of room temperature vulcanising silicone adhesives for high temperature aerospace applications. Statisches Verhalten und Dauerfestigkeitsanalyse von vulkanisierten Silikonklebstoffen für Luftfahrtanwendungen bei hohen Temperaturen. Mater Werkst 2010;41:325–35.
[66] Banea MD, da Silva LF. Mechanical characterization of flexible adhesives. J Adhes 2009;85:261–85.
[67] Silva M, Marques E, Silva L. Behaviour under impact of mixed adhesive joints for the automotive industry. Lat Am J Solid Struct 2016;13:835–53.
[68] Karachalios EF, Adams RD, da Silva LFM. Single lap joints loaded in tension with high strength steel adherends. Int J Adhesion Adhes 2013;43:81–95.
[69] Nunes S, Campilho R, Da Silva F, De Sousa C, Fernandes T, Banea M. Comparative failure assessment of single and double lap joints with varying adhesive systems. J Adhes 2016;92:610–34.
[70] Barbosa A, da Silva L, Oechsner A. Effect of the amount of cork particles on the strength and glass transition temperature of a structural adhesive. Proc IME J Mater Des Appl 2014;228:323–33.
[71] Goglio L, Rossetto M, Dragoni E. Design of adhesive joints based on peak elastic stresses. Int J Adhesion Adhes 2008;28:427–35.
[72] Timoshenko SP, Goodier JN. Theory of elasticity. third ed. McGraw-Hill, Inc.; 1970.
[73] Zhang Y, Noda NA, Takaishi K, Lan X. Effect of adhesive thickness on the intensity of singular stress at the adhesive dissimilar joint. Jounal of Solid Mechanical and Material Engineering 2010;4(10):1467–79.
[74] Carpenter WC, Byers CA. A path independent integral for computing stress intensities for V-notched cracks in a bi-material. Int J Fract 1978;35:245–68.
[75] Zhang Y Y, Noda NA, Wu P, Duan ML. A mesh-independent technique to evaluate stress singularities in adhesive joints. Int J Adhesion Adhes 2015;57:105–17. Corrigendum of authorship "A mesh-independent technique to evaluate stress singularities in adhesive joints". International Journal of Adhesion and Adhesives, Vol. 60, p.130, 2015.